Ocean-based Negative Emission Technologies

OCEAN NETs

Deliverable Title	**D5.8: New/refined parameterizations for modelling ocean alkalinization effects on biogeochemistry and plankton dynamics**
Lead	GEOMAR
Related Work Package	WP 5
Related Task	Task 5.2 (revised Task 5.5)
Author(s)	Markus Schartau
Support	Markus Pahlow, Tronje Kemena, Vanessa Lampe, Jan Taucher, Miriam Seifert (AWI)
Prieto Dissemination Level	Public
Due Submission Date	31.12.2023
Actual Submission	03.05.2024
Project Number	869357
Start Date of Project	01. July 2020
Duration	42 months (30 months funded by EU)

Abstract:
In this report the potential effects of pulsed ocean alkalinity enhancement (OAE) on plankton growth dynamics, efficacy and carbon dioxide removal (CDR) are simulated at an oligotrophic site nearby the Canary Islands (Spain). Parameterizations of how phytoplankton and bacterial growth respond to variations in carbonate chemistry are introduced and applied. The model resolves vertical profiles within a 420 km^2 area of OAE, and within a $2.05 \cdot 10^5$ km^2 surrounding region. Both areas are connected and lateral dispersion causes a horizontal exchange of chemical and biological tracers. The analysis comprises 32 pulsed OAE scenarios of varying intensities and frequencies of alkalinity addition. The intensities of OAE are derived as fractions of total CaO available for OAE in Europe, from 0.05 % (low), 0.1 % (moderate), 0.2 % (high) and 0.4 % (extreme). These four intensities are co-varied with four frequencies of OAE: monthly, seasonal, annual-winter, and annual-summer deployments. The study shows how much the frequency of the OAE influences the efficacies determined locally and remotely. The model results also provide some first insight of potential OAE effects on biological production.

This project has received funding from the European Union's Horizon 2020 research and innovation programme under grant agreement number 869357.

Document History

Date	Version	Description	Name/Affiliation
03.05.2024	1.0	First submitted version	Markus Schartau / GEOMAR Kiel

List of abbreviations, acronyms and definitions

CaO	Calcium oxide (quicklime)
$CaCO_3$	Calcium carbonate
CO_2	Carbon dioxide
$\mathbf{CO_3^{2-}}$	Carbonate
CDR	**C**arbon **d**ioxide **r**emoval
DCM	**D**eep **c**hlorophyll-*a* **m**aximum
ESTOC	**E**uropean **S**tation for **T**ime-Series in the **O**cean of the **C**anary Islands
EEZ	**E**xclusive **e**conomic **z**one
H^+	Hydrogen (proton)
$\mathbf{HCO_3^-}$	Bicarbonate
MLD	Mixed layer depth
NBP	**N**et **b**acterial **p**roduction
NETs	**N**egative **e**mission **t**echnologies
NPP	Net primary production
Ω_a	Aragonite saturation state
OAE	**O**cean **a**lkalinity **e**nhancement
oppla	**Op**timality-based **pla**nkton ecosystem model
PIC	**P**articulate **i**norganic **c**arbon
PLOCAN	Oceanic Platform of the Canary Islands
SSP	**S**hared **S**ocioeconomic **P**athways (climate scenarios / future projections)

List of figures

List of tables

1. Introduction

Context

OceanNETs is a European Union project funded by the Commission's Horizon 2020 program under the topic of Negative emissions and land-use based mitigation assessment (LC-CLA-02-2019), coordinated by GEOMAR Helmholtz Centre for Ocean Research Kiel (GEOMAR), Germany.

OceanNETs responds to the societal need to rapidly provide a scientifically rigorous and comprehensive assessment of negative emission technologies (NETs). The project focuses on analyzing and quantifying the environmental, social, and political feasibility and impacts of ocean-based NETs. OceanNETs will close fundamental knowledge gaps on specific ocean-based NETs and provide more in-depth investigations of NETs that have already been suggested to have a high CDR potential, levels of sustainability, or potential co-benefits. It will identify to what extent, and how, ocean-based NETs can play a role in keeping climate change within the limits set by the Paris Agreement.

1.1 Purpose and scope of the deliverable

The results of the model simulations presented here provide new insights into the quantitative relationships between the intensity and frequency of ocean alkalinity enhancement (OAE) within a small region and their effects on the widespread carbon dioxide (CO_2) uptake in a larger spatial area around the site of alkalinity input. The major aim of this task is to provide and test parameterizations of phytoplankton and bacterial growth that are sensitive to changes in the carbonate chemistry, in particular to changes in pH (or hydrogen proton concentration). Optimal parameter estimates are provided and applied for assessing the potential impacts of OAE on the lower trophic plankton dynamics under typical ocean conditions, at a site where oligotrophic conditions prevail and the overall net primary production rates (NPP) remain low throughout the season. The selected region for modelling such impacts are the oligotrophic areas at and around the European Station for Time-Series in the Ocean of the Canary Islands (ESTOC), where changes of the oceanographic (hydrographic) as well as biogeochemical conditions are monitored. Of particular interest are the strength (magnitude) of change in plankton biomass in association with the different intensities and frequencies of OAE, as well as the characteristic time scales involved, e.g. of recovery in the presence of lateral dispersion and vertical turbulent mixing.

In addition to the evaluation of short-term, pulsed disturbances of carbonate chemistry on primary production and bacterial growth, the following questions are also addressed:

i) How does the frequency of yearly repeated OAE affect the annual CDR and efficacy locally and remotely?
ii) At which year, for a given start and intensity of OAE, would the CDR be similar to the emissions of 50 000 people within the European Union (EU) (population of a medium-sized city in Europe)?
iii) How is CDR affected in case of secondary aragonite precipitation and sinking of particulate inorganic carbon (PIC)?

1.2 Relation to other deliverables

This OceanNETs study represents a massive extension of the earlier model analyses described in **D5.3**. The renewed modeling approach closes more than before the gap between the large-scale model simulations considered in **WP4** and the findings from experimental work on the growth dynamics of plankton, including bacteria. For the study presented here, information from the modeling approach described in **D4.5** (Seifert et al., Alfred-Wegener-Institute, Bremerhaven) was taken into account. An extremely important and valuable dataset, developed and distributed as part of this OceanNETs consortium, informs about the potential quantity of quicklime (calcium oxide, CaO in Gt yr^{-1}) available in the EU for OAE. These data were provided by Tommi Bergman and Antti-Ilari Partanen (Bergmann, et al. 2024) from the Finnish Meteorological Institute, Helsinki. Their cases specify the potential excess capacities in the lime and cement industry, projected for Europe (as well as for the United States and China) up to the year 2100, which form the basis for the different intensities of the OAE investigated in this modeling study. The reported preliminary outcomes from **D5.6** provided valuable insights and helped refining the previous model setup of **D5.3**, in particular with respect to the necessity of resolving cases of potential solid carbonate precipitation of aragonite to form PIC in the model simulations (e.g. see Hartmann et al., 2022), above a critical aragonite saturation state (Ω_a), which may severely impairs the OAE and thus prevents further CDR.

2. Model setup for pulsed OAE and parameterizations of responses in plankton dynamics and biogeochemistry to OAE

2.1 Motivation and background information

The special feature of this study is that a pulsed OAE is explicitly resolved here, which leads to strong changes in the carbonate chemistry within a short period of time and is thus also accompanied by a strong perturbation of the planktonic ecosystem. Assessing the extent of this short-term disturbance is an essential part of the study. This topic was already addressed in **D5.3**, but was only examined for a short period of a few years. Furthermore, the question arose as to the transferability of the previously obtained model results. At the last annual OceanNETs meeting (in Hamburg, September 2023), it was discussed to what extent the lateral dispersion of the pulsed OAE events could have on the interpretability of the results and whether my results could simply be scaled up. My own scepticism about upscaling has led me to fundamentally revise the approach. The idea that emerged from the discussion was to extend the model to differentiate between a local effect at the site of the OAE and the effects on a larger surrounding area. In addition to these model changes, a pH sensitivity of bacterial growth was also introduced, which I had already put forward as an important consideration. Apart from the changes with regard to the spatial distinctions, the parameterizations of the possible growth changes in phytoplankton and bacteria were revised or newly implemented.

First, the areas and their extent are described. Then the individual scenarios of the pulsed OAE are defined. The parameterizations that determine the sensitivities of the growth rates are then specified, including their parameter values. These parameterisations and their respective parameter values can be easily adopted for other modelling studies where pulsed OAE are subject

to investigations. Prior to the presentation of the simulation results of the OAE scenarios, relevant results of the two (baseline) reference solutions are shown, which are based on the climate scenarios (SSP126) and (SSP370), according to O'Neill et al. (2016),
see also https://www.dkrz.de/en/communication/climate-simulations/cmip6-en/the-ssp-scenarios:

a) SSP370: A newly introduced scenario, with an additional radiative forcing of 7 W m^{-2} by the year 2100, making it a scenario of the upper-middle part of the full range of scenarios.

b) SSP126: In this scenario the additional radiative forcing reaches 2.6 W m^{-2} by the year 2100. It is a remake of the optimistic scenario RCP2.6 that is compatible with reaching the 2 °C target, while climate protection measures are assumed to be taken.

2.2 Location and spatial distinctions and scaling of simulation areas

Similar to the location chosen for the simulations described in **D5.3,** the basic site of OAE is assumed to be off-shore of the Canary Islands, but still within the exclusive economic zone (EEZ) of Spain. This chosen, hypothetical, site for OAE corresponds to the European Station for Time-Series in the Ocean of the Canary Islands (ESTOC), at 29.04°N, 15.50°W. Although an actual implementation of OAE can be ruled out at this particular site, the oceanic conditions there are representative of the oligotrophic conditions that extend far into the international waters beyond the Canary Islands. As previously argued in **D5.3**, the advantage here is that measurement data are available and scientific studies on the biogeochemistry and plankton at ESTOC had been conducted there, including modelling analyses (e.g. Neuer et al, 2007; González-Dávila, et al. 2010; Yumruktepea et al., 2020). These studies helped constraining the model results and their outcomes are used to assess the representativeness of the reference solutions used in this study.

With the extended model version, two areas (A1 and A2) are considered, with A1 representing the area of OAE and A2 being a much larger surrounding region. Both areas are connected and lateral dispersion of water masses (lateral diffusion) causes the chemical tracers and biological variables to be exchanged horizontally. For the turbulent vertical mixing, it is assumed that there is no difference between the areas and differences are only associated with the two climate scenarios, SSP126 and SSP370 respectively. For a meaningful upscaling, which is the primary objective of distinguishing between a local and a surrounding area, the relative proportions of the extents of A1 and A2 are relevant, as shown in Figure (1):

- **A1**: This area is subject to OAE. It covers an area of 420 km^2, based on the following considerations. If a ship is considered with an average speed of 18.5 km h^{-1} (≈ 10 knots), then it would travel a distance of 444 km per day, which could be split up into 20 parallel transects that are 1 km apart. If each individual transect has a distance of 21 km, then a 20 km x 21 km (420 km^2) area can be covered during 24 hours. In this case the parallel transects are 1 km apart. If these parallel transects are slightly offset and repeated, it would take a three days period for OAE, with tracks being no more than 333 m (1/3 km) apart, which would provide almost homogeneous coverage of alkalinity addition. Thus, an area of such size is realistic in terms of OAE to be well achieved within a three days period. Accordingly,

each OAE event resolved in the model, no matter which frequency of OAE is considered, has a duration of three days.

- **A2**: The outer region A2 is larger than A1 by a factor of ≈ 489, which allows for some reasonable upscaling. A2 covers a region of $2.05 \cdot 10^5$ km², and the scaling factor A1:A2 is $2 \cdot 10^{-3}$ accordingly. In other words, A1 accounts for only 0.2 % of the total area of A2. It is emphasized that the simulated area of A2 does not actually include (incorporate) the area A1 for reasons of mass and volume conservation, which is guaranteed in this model setup.

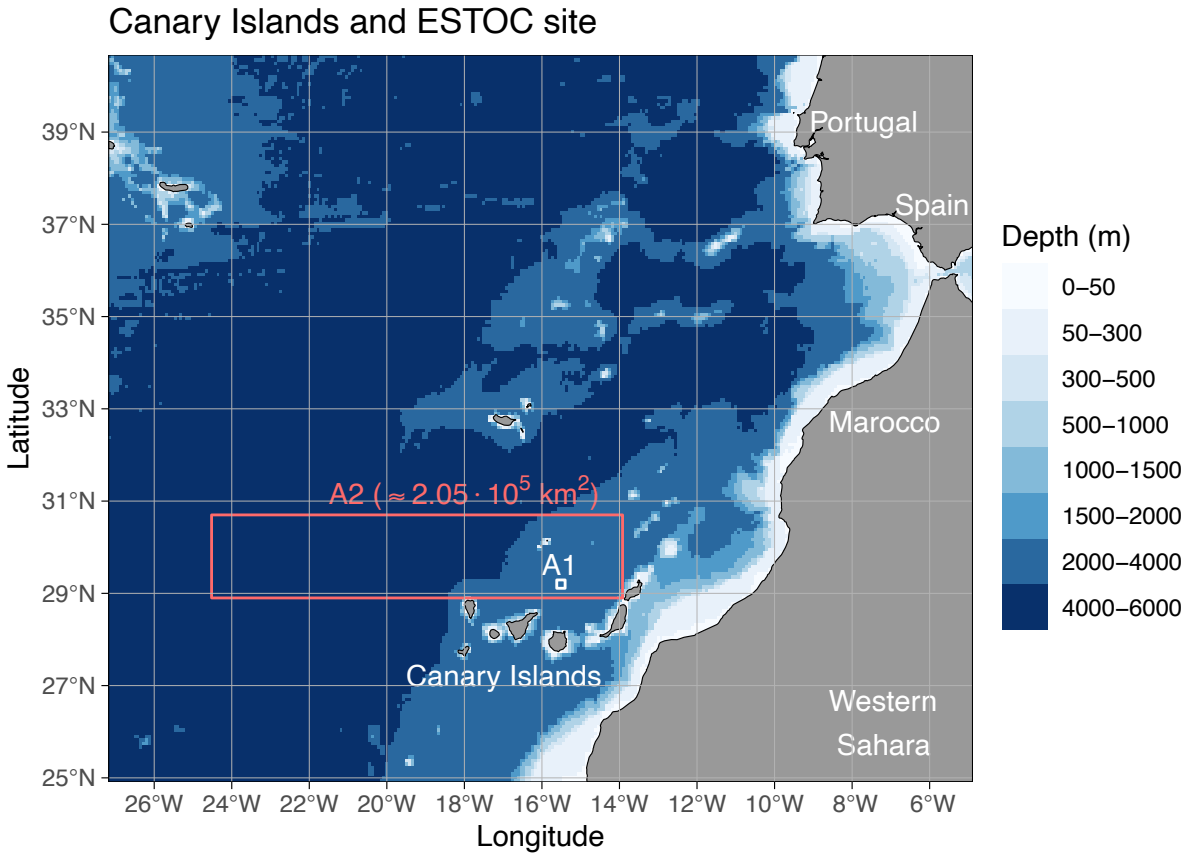

***Figure 1**: Area map of OAE at ESTOC site (29.04°N, 15.50°). The area A1 covers a 420 km² region that is here assumed to be subject to OAE. The outer region A2 extends to $2.05 \cdot 10^5$ km². The shown outer limits of A2 only exemplify the proportions of this domain in relation to A1, but with the relative proportions A1:A2 = $2 \cdot 10^{-3}$ (scaling factor of 0.2 %) being correctly depicted here.*

2.3 Physical conditions, vertical and lateral mixing of tracer concentrations

In general, the concentration of either a chemical or biological tracer (S) and its rate of change (dS/dt) is determined for A1 and A2 being coupled (connected), similar to that of a three-dimensional coupled circulation model, although an explicit representation of advection is neglected. The vertical mixing varies with time and depth, using the vertical diffusion coefficient derived from the results of the three-dimensional simulations with the FOCI (Flexible Ocean and Climate Infrastructure) model, operated at GEOMAR. Additional results from these FOCI simulations are used as physical environmental boundary conditions, including wind speed, temperature, salinity, surface irradiance, and atmospheric carbon dioxide (CO_2), which were

kindly made available by Tronje Kemena (personal communication). It is noted that these physical boundary conditions differ for the two climate scenarios SSP126 and SSP370. For this reason, two separate reference solutions of the biogeochemical tracers are considered when it comes to the analyses of the different OAE scenarios presented herein. It is assumed that the horizontal mixing between A1 and A2 is time-invariant, while imposing a lateral diffusion coefficient of $K_h = 2.5 \cdot 10^3$ $m^2\ s^{-1}$, which is typical for this particular region (Zhurbas, et al., 2014):

$$(1) \qquad \frac{dS}{dt} = \text{sms} + K_h \cdot \frac{\partial^2 S}{\partial x^2} + \frac{\partial}{\partial z}\left(K_v(z)\frac{\partial S}{\partial z}\right)$$

with sms representing the source minus sink terms of the state variable S, as introduced by the biogeochemical and plankton ecosystem dynamics. Figure (2) shows the most relevant differences between the two climate scenarios at the region of interest. The progressive and gradual shallowing of the mixed layer depth (MLD) in the SSP370 scenario reflects one major important difference, if compared with the SSP126 scenario. This temporal development is associated with the, also important, trend seen in atmospheric CO_2. From previous comparisons (see **D5.3**), the MLDs derived from FOCI simulations are regarded as being representative for the ESTOC site, with a good agreement with the observations of hindcast model results. The simulated winter MLDs mostly range between 100 and 200 m, hardly exceeding 200 m in some years. The shallowest mixing depth resolved by the model is MLD = 13 m, which is typically reached in the summer months.

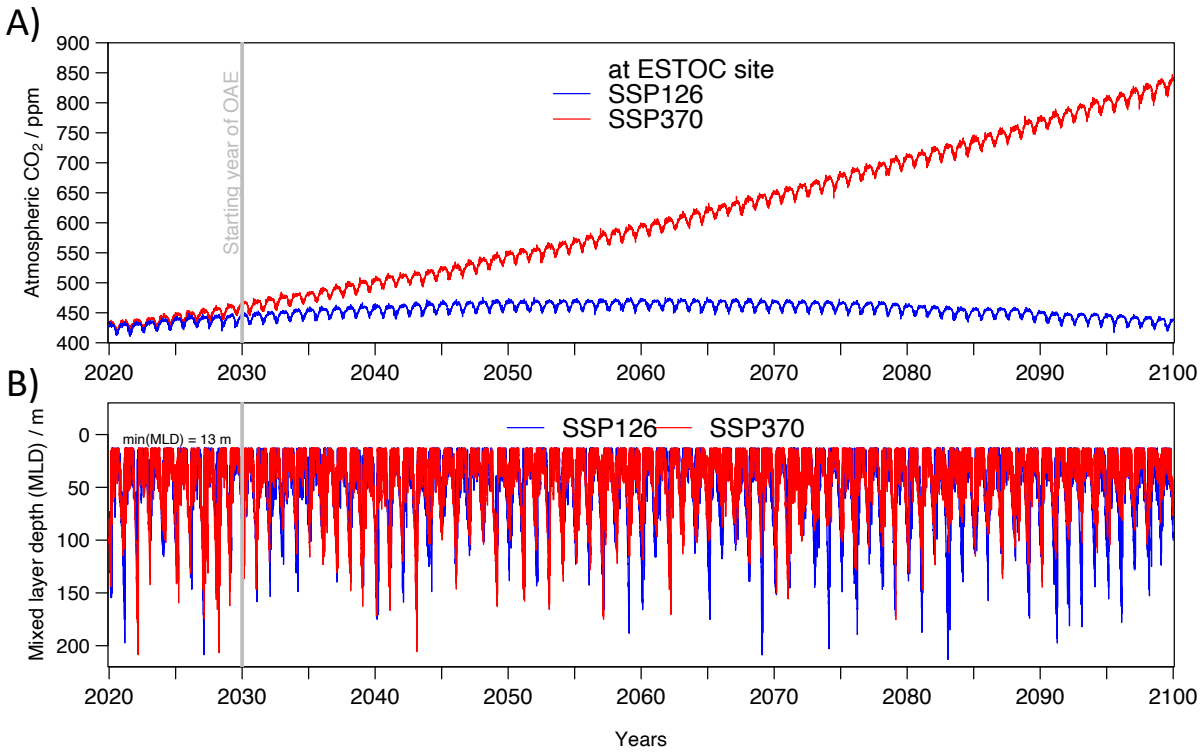

Figure 2: Climate scenarios (SSP126 and SSP370). A) Atmospheric CO2 concentrations for the two climate scenarios, SSP126 (blue line) and SSP370 (red line) respectively. The gray vertical line indicates the time when OAE is assumed to start in the simulations. B) Mixed layer depth (MLD) that varies on seasonal scale, but also shows substantial interannual variability. The SSP370 (red line) scenario exhibits a gradual decrease of MLD with time, if compared with SSP126 (blue line). The minimum MLD is approximately 13 m, whereas the maxima hardly exceed depths of 200 m.

2.4 Specification of the ocean alkalinity enhancement (OAE) scenarios

A total of 32 different OAE scenarios are examined, which differ in their intensity and frequency as well as in their physical environmental conditions due to the two climate scenarios SSP126 and SSP370. In accordance with the climate scenarios, two additional model runs serve as reference simulations without any OAE. The calculations of alkalinity enrichment and CDR are set in relation to these respective reference results of SSP126 and SSP370, as well as the relative changes in the biological state variables.

The intensities of OAE are assumed to be proportional to the quantity of quicklime (calcium oxide, CaO in Gt yr^{-1}) available in the EU for OAE, as provided and distributed within WP4 by Tommi Bergman and Antti-Ilari Partanen (Bergmann, et al. 2024) from the Finnish Meteorological Institute, Helsinki. They indicate the potential overcapacities in the lime and cement industry that are projected up to the year 2100 for the European Union. These data are separated by the assumed starting year of OAE, and are distinguished according to a low and high potential of excess quicklime availability. For the purposes of the study presented here, the year 2030 is considered to be the start of the OAE, and the lower case of excess availability of quicklime was used as the basis for the derivation of the intensities of OAE. The area of OAE at the oligotrophic site of ESTOC (A1 = 420 km^2) is approximately 0.1 ‰ of the total deployment region assumed for all excess quicklime available (≈ $4.426 \cdot 10^6$ km^2). Therefore, an appropriate intensity of OAE for A1 should be in the order of 1 ‰ in relation to the total excess availability of quicklime.

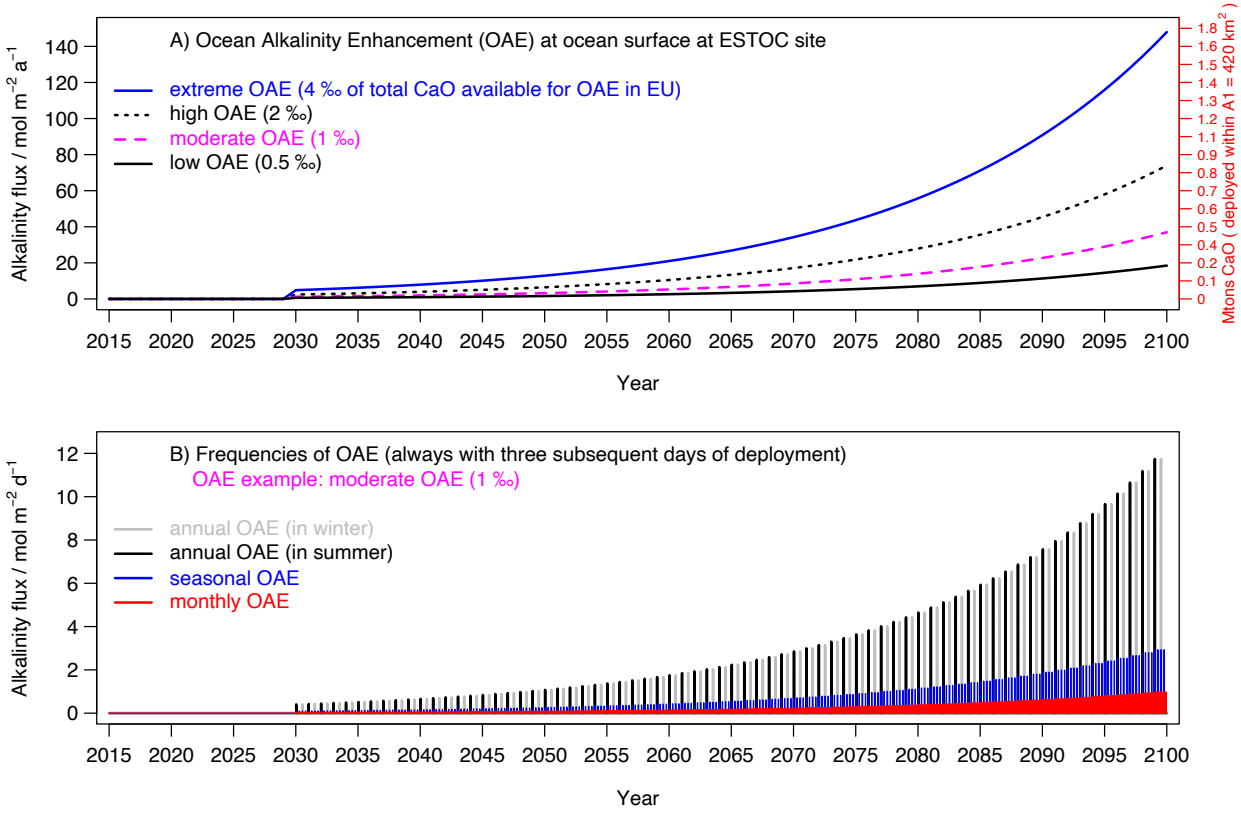

Figure 3: Scenarios of ocean alkalinity enhancement (OAE) at ESTOC site within an area of 420 km². A) Intensities of OAE, with respective yearly surface alkalinity fluxes in units [mol m^{-2} a^{-1}] and the corresponding mass of CaO in Mega-tons. First year of OAE is 2030. B) Frequencies of OAE, with the yearly alkalinity addition events being differently distributed throughout the year: monthly, every three months (seasonal), once per year (annual) in winter and in summer.

Four different intensities are assumed for alkalinity addition at the ocean surface, derived as per mille (‰) fractions of the in Europe available quicklime, converted from annual Gt of CaO to a yearly alkalinity flux in units of mol m^{-2} a^{-1} (Figure 3A), with i) low = 0.5 ‰, ii) moderate = 1.0 ‰, iii) high= 2.0 ‰, and iv) extreme = 4.0 ‰ of total available CaO.

Another distinction is to distribute the annually available amount of TA over certain periods during the year. Thus, different frequencies of OAE are considered. If the same amount of alkalinity addition is restricted to happen once in a year, then the associated perturbation of the carbonate system and thus of the biological condition will be more intense than for a rather gradual and smooth addition, like for an alkalinity addition every month. Four frequencies of OAE are considered here: i) monthly, ii) seasonal, and once per year deployments, distinguished between iii) annual winter and iv) annual summer additions, see example for OAE of moderate intensity in Figure (3B). A separation of the annual OAE is meaningful, because vertical mixing conditions are very different in winter than in summer. As already explained in section 2.2, each OAE event, regardless of its frequency, extends over a period of three days.

Overall, we have four frequencies assigned to four different intensities (16 simulations) for every of the two climate scenarios (SSP126 and SSP370), which makes a total of 32 simulation runs. In addition, a reference solution is required for every climate scenario. In the end, results of 34 simulations enter this OceanNETs model analysis.

2.5 Parameterizations of phytoplankton and bacteria growth responses to changes in carbonate chemistry

Similar to the applications in **D5.3**, the basic plankton ecosystem model is the OPPLA (OPtimality-based PLAnkton) ecosystem model, which has been developed and constantly refined by Markus Pahlow at GEOMAR (e.g. Pahlow et al., 2013; Grossowicz and Pahlow, 2024). In OPPLA, first-order principles are applied, such as optimal resource allocation, which allow meaningful responses of plankton growth to variations in environmental conditions. OPPLA resolves details of variations in intracellular ratios of carbon-to-nitrogen, nitrogen-to-phosphorus and chlorophyll-to-carbon, which are not considered by most Earth system models.

Two functional responses have been introduced to OPPLA for this study. These functions are normalized and are thus dimensionless and they modulate the apparent growth rates of the phytoplankton and of the bacteria under varying conditions of the carbonate system. First, some brief background information about the response functions of the CO_2 effects on the phytoplankton is provided. Then, the response function used in this study is described, together with the corresponding parameter estimates. Then, a response function for the assimilation of carbon and of nitrogen is specified for bacterial growth.

In **D4.5** a response function of the CO_2 effect on algal growth is described that has been applied in Seifert et al. (2022) and that builds on the parameterization proposed by Bach et al. (2015):

$$f_{\mathrm{rel}} = \frac{\mu}{\mu^*} = \frac{a \cdot [\mathrm{HCO_3^-}]}{b + [\mathrm{HCO_3^-}]} - \exp\left(-c \cdot \left[\mathrm{CO_{2(aq)}}\right]\right) - d \cdot 10^{-\mathrm{pH}} \quad (2)$$

which considers the bicarbonate concentration $[HCO_3^-]$ and seawater carbon dioxide concentration $[CO_{2(aq)}]$ explicitly, together with changes in pH. The four parameters (a, b, c, d) were estimated in the study of Seifert et al. (2022) for calcifying coccolithophores, silicifying diatoms, as well as for small phytoplankton. After consultation, my plan was to adapt this function for my OAE scenarios as well, not least for reasons of comparability. I derived parameter estimates for Equation (2) that represent the mean of the responses obtained for the diatoms and the small plankton (not shown here). I note that the mean response is not simply determined by averaging the individual parameter values of the diatoms and small phytoplankton.

Using this equation, it was by no means possible to achieve a complete series of model runs for all 32 OAE scenarios. Given the short-term, potentially intense, perturbations of the carbonate system due to the alkalinity additions, this function can occasionally become negative. This in turn can cause instabilities and may end up with model simulations to crash or fail. In retrospect and based on the experience gained here, this additive formulation of Equation (2) can lead to undesirable problems under conditions in which the carbonate system becomes severely perturbed, as is the case in the simulations applied here. For this reason, I returned to the somewhat newer parameterization proposed by Paul and Bach (2020), where similar problems had not occurred. However, to achieve comparability, this time I used the averaged response (of the diatoms and the small phytoplankton) to again obtain optimal parameter estimates, but for the relationship of Paul and Bach (2020):

(3)
$$f = \frac{\mu}{\mu^*} = \left(1 - \frac{[H^+]}{[H^+]^*}\right)^n \cdot \frac{[H^+]}{[H^+] + c_M \left(1 - \frac{[H^+]}{[H^+]^*}\right)^m}$$

The parameterization of Paul and Bach (2020) builds entirely on the proton hydrogen concentration $[H^+]$. Figures (4) and (5) show the individual responses in the normalised growth rates ($\frac{\mu}{\mu^*}$) to variations of the major components of the carbonate system, of the relationship used in Seifert et al. (2022), the mean response of their results and the corresponding fit obtained for Equation (3). The parameter estimates obtained and applied here are given in Table (1).

The potential maximum bacterial growth rate is assumed to depend on the enzymatic activity, which is not only sensitive to the ambient temperature but also to pH. For any given temperature, the maximum enzymatic activity has an optimum at some specific pH value (Bisswanger 2014). There are hardly any measurements of enzyme activities for oceanic conditions, and if there are, it is not clear how sensitive they are to changes in pH. The study of Piontek et al. (2015) documents a nearly linear dependency between hydrolytic extracellular enzyme activities and the production of a natural bacteria population, and it provides experimental evidence of the response of enzymatic activities to variations in seawater pH. In their (on board) experiments the activities of two hydrolytic enzymes were analyzed, leucine-aminopeptidase (for nitrogen-enriched amino acids) and beta-glucosidase (for carbohydrates) respectively. Although their experiment was primarily aimed at the changes due to reduced pH values (ocean acidification), their measurements also include the case of increased pH values, as they can occur under conditions of pulsed OAE. Their measurements show a reduction in enzyme activities if pH exceeds the natural values. They revealed pH optima around 6.7 for leucine-aminopeptidase and

below pH of 6.0 for beta-glucosidase. For the purpose of transferability to the model study, their measured values were normalized, i.e. the measured rates ($V_{C,N}$) were divided by the rates found under the in-situ pH conditions ($V^*_{C,N}$). These normalised data were then used to fit a bell-shaped functional response function that is assumed to be similar for the utilisation of the carbohydrates (C) and the amino acids (N) by the bacteria, but with different parameter values respectively. A root mean square error minimisation was conducted to derive optimal parameter estimates for the following functional response:

$$f_{C,N}^{(bac)} = \frac{V_{C,N}}{V^*_{C,N}} = A_{C,N}^{(max)} \cdot \exp\left(-\frac{(pH - o_{C,N})^2}{w^2}\right) \quad (4)$$

with $A_{C,N}^{(max)}$ being the amplification factor for C and for N respectively. The corresponding parameters $o_{C,N}$ are the pH optima (for C and for N). The parameter w represents the width of the response function, which is assumed to be identical for C and for N. Figure (6) shows the respective response functions as well as the normalized data.

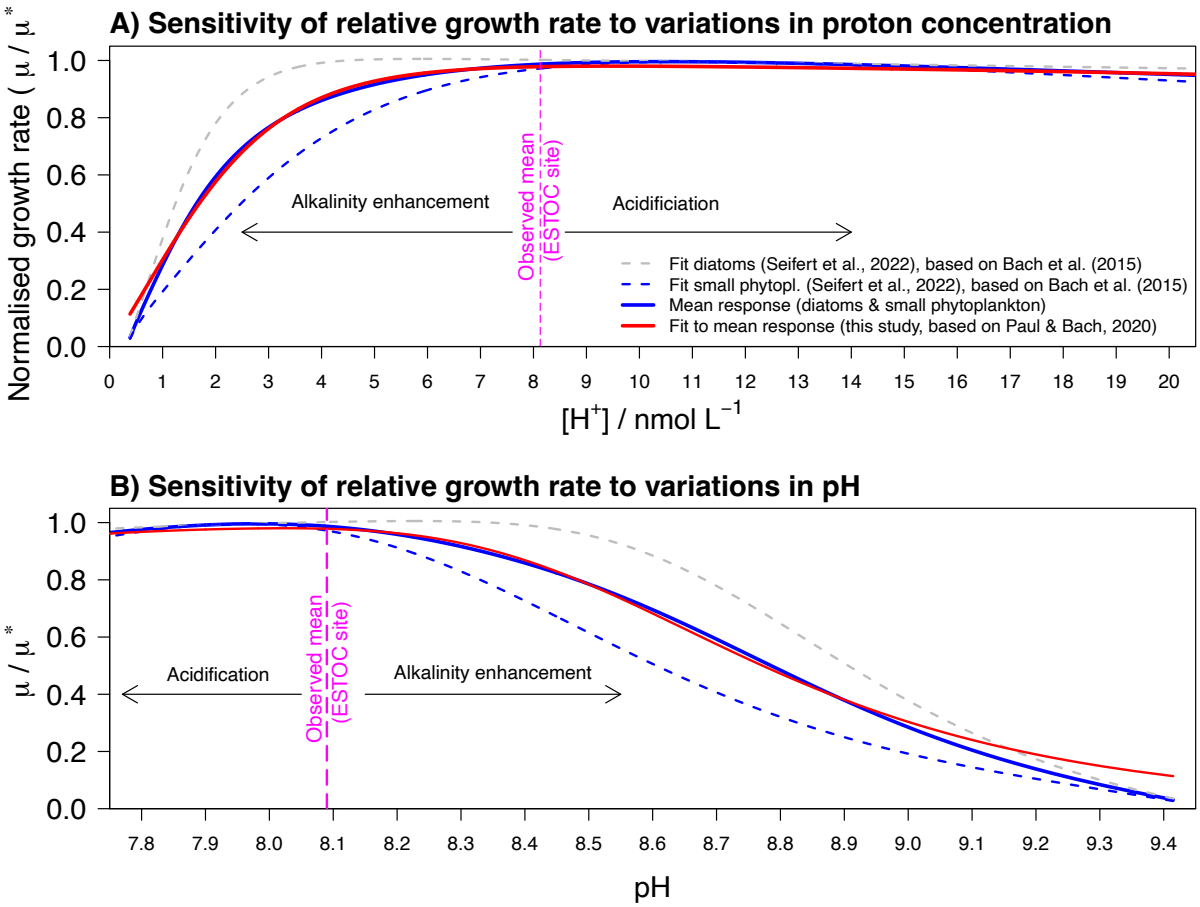

Figure 4: Sensitivities of phytoplankton growth rates to pH. A) Responses of phytoplankton growth rates to variations in proton (hydrogen) concentration, for diatoms and for small phytoplankton, as derived in Seifert et al., (2022) (dashed lines), the associated mean response (blue line) and the corresponding fitted response, based on the parameterization of Paul and Bach (2020). B) the same relationships as in A) but shown as a function of the pH value.

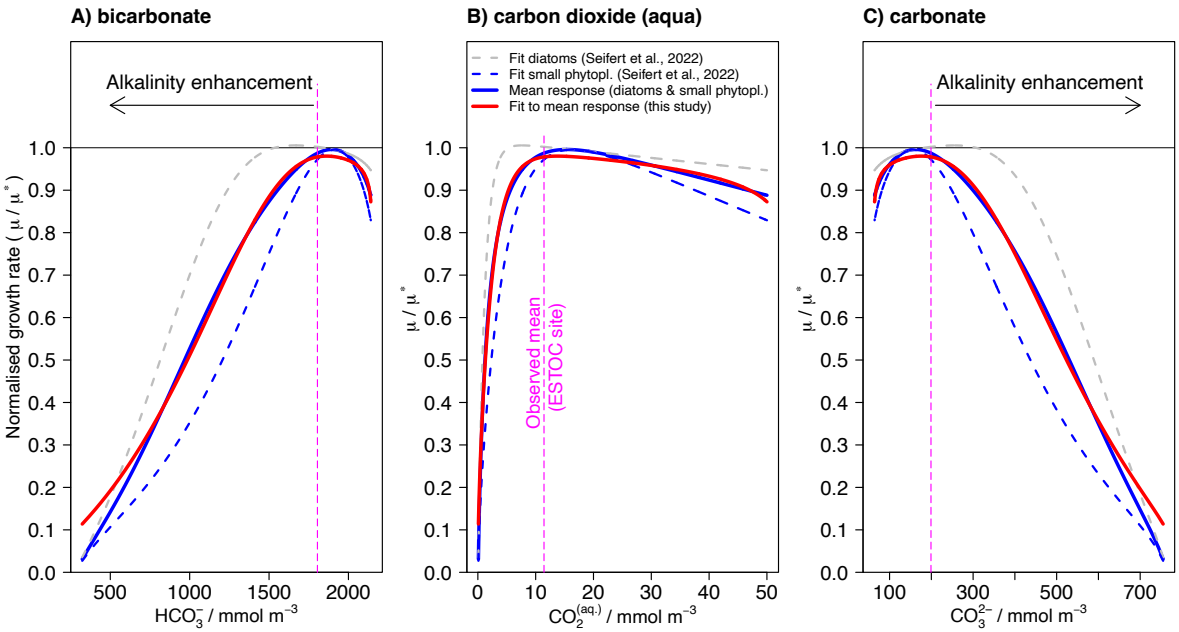

Figure 5: Sensitivities of phytoplankton growth rates to variations of the components of the carbonate system. Responses of phytoplankton growth rates to variations in A) bicarbonate concentration, to B) seawater carbon dioxide, and to C) carbonate ion concentration. Dashed lines represent fits for diatoms and for small phytoplankton derived in Seifert et al., (2022). The solid blue line represents the mean response of the diatoms and small phytoplankton. The red line depicts the response fitted to the mean (blue line), but using the parameterization of Paul and Bach (2020) instead.

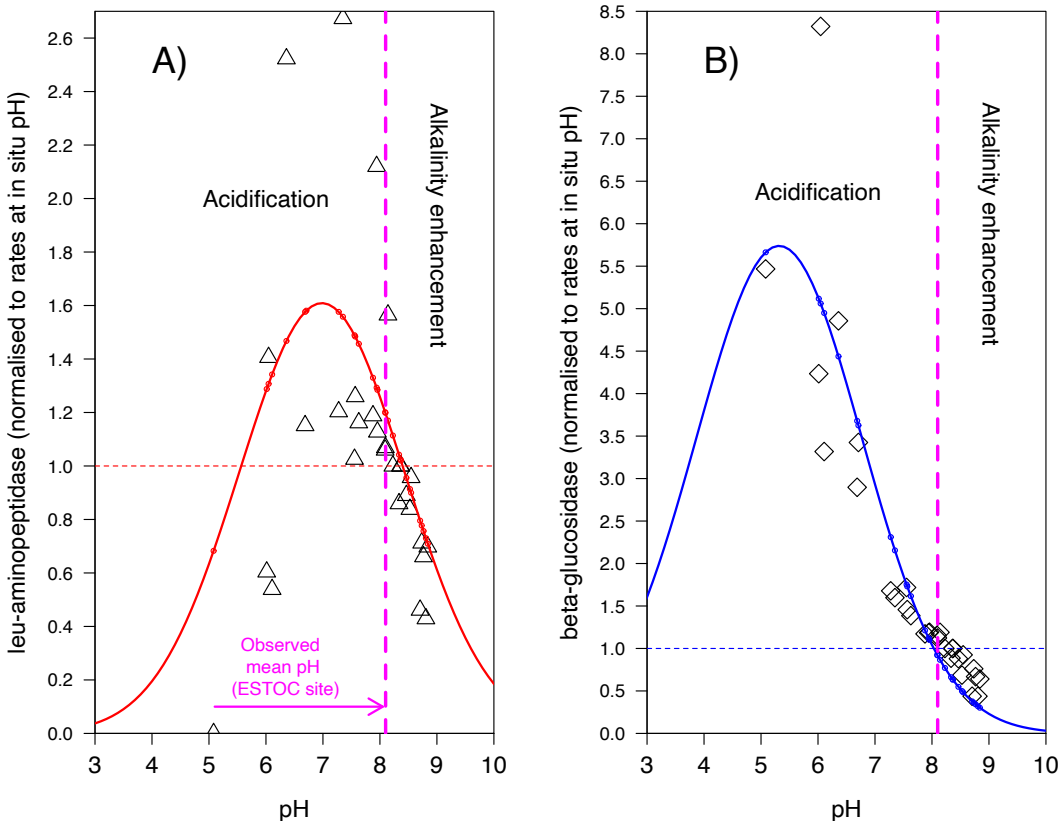

Figure 6: Sensitivities of bacterial enzymatic activities to variations in pH. A) Normalized rates of leucine-aminopeptidase activity for varying seawater pH conditions. The red line depicts the root mean square fit of Equation (4) to the normalized data of Piontek et al. (2015). B) Normalized rates of beta-glucosidase activity and the corresponding fit (blue line). The data and the fitted response function resolve a clear reduction of the enzymatic activities when pH levels are above those measured in-situ. The vertical dashed line (magenta) indicates the typical pH values found at the ESTOC site.

***Table 1**: Optimal parameter estimates for functional responses of growth to variations in pH. The response function for phytoplankton growth (Equation 3) is based on the relationship proposed by Paul and Bach (2020) and the corresponding parameter estimates represent the fit against the mean response function of Seifert et al. (2022). The pH-response function of bacterial growth (Equation 4) was fitted against normalized data of Piontek et al. (2015).*

Response function (Equation 3) for phytoplankton growth			**Response function (Equation 4) for bacterial growth**	
Name	Value	Unit	Name	Value
$[\mathbf{H}^+]$	$3.184 \cdot 10^{-8}$	mol kg^{-1}	$A_C^{(pot)}$	5.739
$\boldsymbol{C_M}$	$3.535 \cdot 10^{-9}$	mol kg^{-1}	$A_N^{(pot)}$	1.609
$\boldsymbol{n}$	0.0478	-	o_C	5.318
$\boldsymbol{m}$	13.61	-	o_N	6.982
			w	2.053

2.6 Model implementation of particulate inorganic carbon (PIC) precipitation

The potential of secondary precipitation during the OAE was highlighted by Hartmann et al. (2022), based on side experiments and it was also observed in a rare case during the post-phase of the OceanNETs Canary Islands mesocosm experiment. According to their findings, it was emphasized that the model simulations should consider such a possibility of precipitation of aragonite, which may not only prevent the effectiveness of OAE, but may also cause the alkalinity to drop below the level that was already reached before precipitation, also referred to as runaway precipitation (Moras et al., 2022). It was pointed out that there is a risk of particulate inorganic carbon (PIC) formation in OAE without an accompanied CO_2 addition, i.e. OAE with CO_2-equilibrated seawater. These concerns were taken seriously in this simulation study and an explicit, although simplified, representation of PIC precipitation has been included in the model. It is regarded as simple, because the precipitation of PIC is treated as an exponential growth process, with a constant rate of 0.1 d^{-1}, starting at some prescribed critical value of the aragonite saturation state (Ω_a). However, the PIC formed is subject to vertical sinking and may therefore export alkalinity to great depths, which may potentially lead to the situation of runaway precipitation. In Schulz et al. (2023), Guide to Best Practices in Ocean Alkalinity Enhancement Research (Oschlies, et al. 2023) and in Moras et al. (2022), different types of PIC precipitation are distinguished, i.e. i) heterogeneous (in the presence of nucleation surfaces such as solid minerals), ii) homogeneous (in the absence of nucleation surfaces), and iii) pseudo-homogeneous (with nucleation surfaces like colloids and organic particles). For the ESTOC site, conditions are assumed that are associated with the presence of solid (e.g. when calcifying algae are abundant) and of organic substances that can both act as nucleation surfaces. This means that the scenario reproduced here can be interpreted as a partially heterogeneous and pseudo-homogeneous precipitation. For the simulations a constant but tiny background of nucleation surfaces is assured via a surface in- and throughflux that maintains a PIC concentration of approximately 0.1 mmol m^{-3} (1.2 µg/L). Once the critical value of Ω_a is reached, the precipitation is initiated, which causes PIC concentrations to increase. All PIC is

subject to sinking and is thus exported to depth. The level of background PIC concentration sets the initial condition for the exponential process of PIC formation. Moras et al. (2022) reported that for Ω_a remaining below 5, it is very unlikely that PIC precipitation occurs. The found PIC precipitation to occur at $\Omega_a = 7$, although this has been attributed to the situation of heterogeneous precipitation. For a critical and rather conservative evaluation of our simulations, a value of 7 is defined as critical Ω_a.

2.7 Model reference solutions

To determine the changes caused by the OAE, it is important to simulate the typical alkalinity (total alkalinity, TA) and dissolved in organic carbon (DIC) concentrations and pH on site. The reference solutions therefore describe all those changes over time that are not caused by OAE. For comparison with observational data, a time period of 10 years prior to the start of OAE is documented here. The chlorophyll-a concentration, net primary production (NPP) and net bacterial production (NBP) are also shown for the entire 81-year period (from 2020 to 2099).
In Figure (7) the data of TA, DIC, pH, as well as sea surface temperature are depicted, as observed during the period between 1995 and 2020, all projected into a single year. These data were kindly made available by Melchor González Dávila (Oceanic Platform of the Canary Islands, PLOCAN) and Magdalena Santana Casiano (personal communication). Model counterparts to the observations, from the years 2020 through 2029, are projected likewise. The variability in the observed TA exceeds the variations in the model simulations (Figure 7A), but the simulated mean TA (2473 mmol m^{-3}) does not reveal any noticeable bias. Some bias, albeit small, can be seen when DIC concentrations are compared, with slightly higher DIC concentrations in the simulation results (Figure 7B). This is due to the fact that the temporal development of the DIC has progressed further in the period after 2020 (ocean acidification) and therefore the concentrations are higher than those from the 25 years period before. Unfortunately, no hindcast model simulations were considered here, and the first five years of model integration (2015 – 2019) are treated as spin-up years. Given the good TA but slightly higher DIC concentrations in the model results, the simulated pH values tend to be slightly lower than in the data (Figure 7C). The range of simulated sea surface temperature (SST), used here as physical condition derived from the FOCI projections, compares generally well, but the seasonal patterns do not fully coincide with the observations (Figure 7D). The SST in the model results appears to be 1° to 2° Celsius lower during October and November. However, comparisons of the mixed layer depths, with data from Yumruktepe et al. (2020), the physical model results do show good general agreement with the observations (not shown here, see also results presented in **D5.3**).

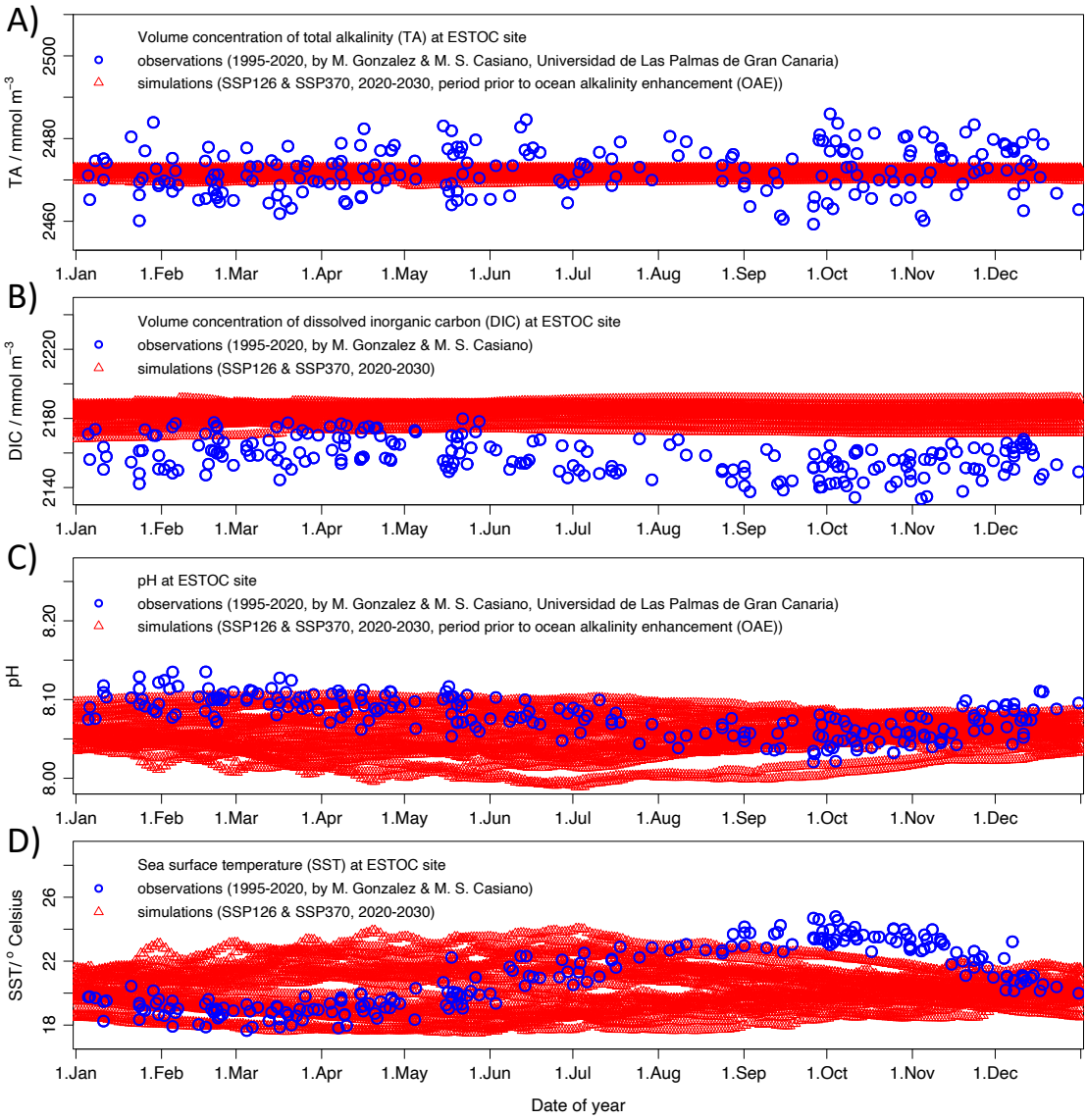

***Figure 7**: Data-model comparison of carbonate chemistry at ESTOC site. A) Total alkalinity (TA), B) Dissolved inorganic carbon (DIC), C) pH, and D) sea surface temperature (SST). Observational data were kindly provided by Melchor González Dávila (Oceanic Platform of the Canary Islands, PLOCAN) and Magdalena Santana Casiano (personal communication).*

The reference solution of the chlorophyll-*a* concentration presented in **D5.3** exhibits short-term maxima that exceed 1.4 mg m^{-3}. This has been corrected and now the simulated maxima in chlorophyll-*a* concentration remain mostly below 1.0 mg m^{-3} (Figure 8). The long term projection shows substantial interannual variability, but the depth of the deep chlorophyll-*a* maximum (DCM) remains fairly stable, typically varying between approximately 80 m and 120 m. For a better comparison with data published by Neuer et al. (2007), the color code has been adjusted in Figure 8B so that it is similar to the published Figure (8C). Simulated and observed DCM agree well, while the simulated chlorophyll-*a* concentration now tends to be lower than observed, rather than too high as it was the case in **D5.3**.

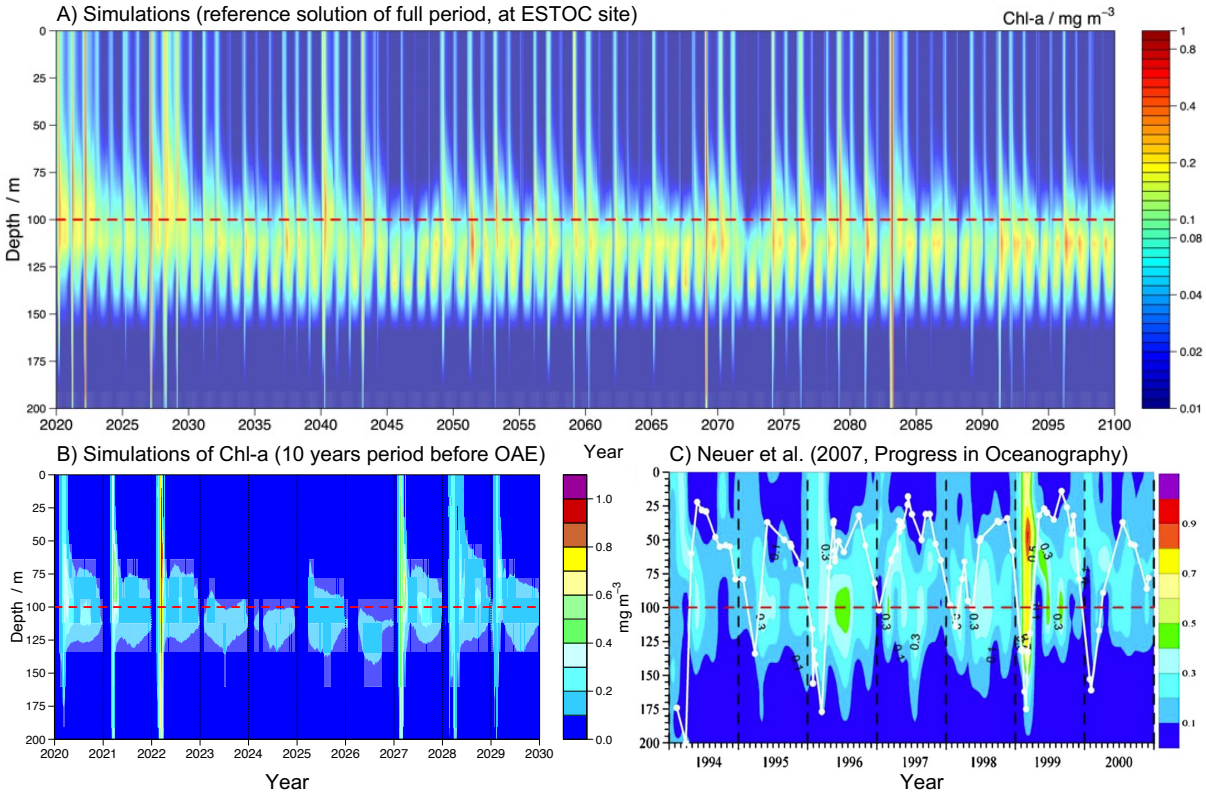

Figure 8: Simulated chlorophyll-a concentrations of the upper 200 m. A) long term projection of the chlorophyll-a concentration, with deep chlorophyll-a maxima (DCM) typically at depths between 90 m and 120 m. B) chlorophyll-a concentration resolved for a ten years period prior to the start of OAE (2020 through 2029), with the color scale refined to match with color scale of C) the figure published in Neuer et al. (2007).

Depth integrated net primary production (NPP) and net bacterial production of the reference solutions are depicted in Figure (9). Typical integrated rates of NNP at the ESTOC site range between 10 and 70 (mmol C) m^{-2} d^{-1} (e.g. Yumruktepe, et al. 2020). In the reference solution, the integrated NPP fall within the same range. In some years the maxima in NPP are above 200 (mmol C) m^{-2} d^{-1} for short period of time. The differences between the scenarios SSP126 and SSP370 do not show a systematic offset or trend up to the year 2090. Clearly, from 2090 on the integrated NPP of the SSP126 scenario are high then in the SSP370, most likely because of the gradual stratification (ocean warming) of the SSP370 climate scenario. While NPP feature a clear seasonal signal along with interannual variability, the seasonal variations of NBP are less pronounced and are actually less expressed than the interannual variability. The latter is substantial. During some periods the integrated NBP can be as high as the NPP or even higher, while most of the time the NBP is about 10 to 40 % of the NPP. Figure (10) shows the NPP and NBP (averages of the two climate scenarios SSP126 and SSP370) resolved over depth. The NPP follows a clear seasonal cycle, with considerable NPP reaching down to 150 m. In contrast to the chlorophyll-*a*, the NPP does not show a maximum at the depth of the DCM. This is due to the fact of the photoacclimation effect resolved by the model, with the chlorophyll-a-to-carbon ratio being higher at the DCM than nearby the surface. The NBP maxima typically occur just below the DCM, below 130 m. As seen before, the interannual variations in NBP are strong.

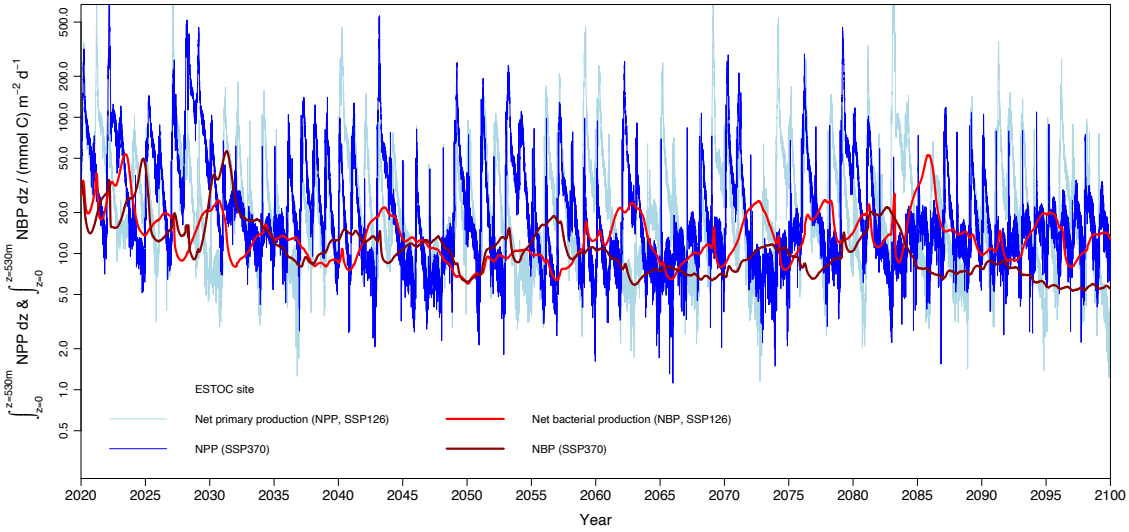

***Figure 9**: Long-term projections of depth integrated (upper 530 m) net primary production (NPP, mmol C m-2 d-1) of SSP126 (lighblue) and SSP370 (blue) and of net bacterial production (NBP) of SSP126 (red) and SSP370 (darkred).*

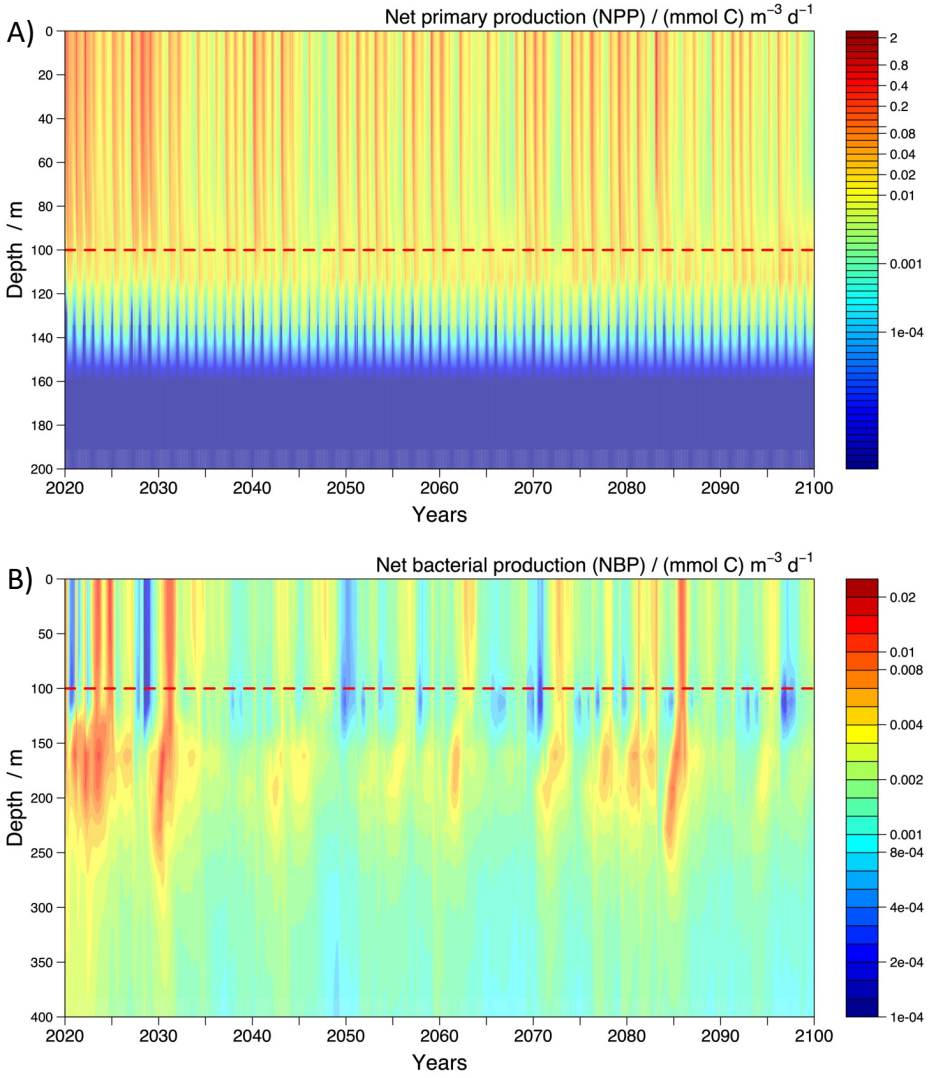

***Figure 10**: Long-term projections of NPP and NBP. A) net primary production (NPP) in (mmol C) m-3 d-1 and B) net bacterial production (NBP) in (mmol C) m-3 d-1. Subplots A) and B) show the averages of the climate scenarios SSP126 and SSP370.*

3. Potential effects of pulsed OAE on biogeochemistry and plankton dynamics under oligotrophic conditions

3.1 Efficacies, pH and CDR of pulsed OAE of different intensities and frequencies

The efficacy, or effectiveness, is a measure of how much CDR is achieved for a given amount of OAE. This can be assessed on an annual basis, where the total additional uptake of CO_2 and the corresponding increase in DIC concentration of a specific year is related to the total amount of alkalinity added in that year. Here, the efficacy is evaluated on a daily basis ($E^*(t)$), mainly for resolving temporal variations of the different types of pulsed, short-term OAE. This informs about the different time scales involved with regard to the lateral dispersion (exchange between A1 and A2) and the air-sea flux of CO_2. For the analyses, the differences to the reference solutions (absence of OAE) in DIC and total alkalinity (TA) are evaluated as follows:

$$E^*(t) = \frac{\int_{z=0\mathrm{m}}^{z=2600\mathrm{m}} (\mathrm{DIC}(t,z) - \mathrm{DIC}_{\mathrm{ref}}(t,z))\ \mathrm{d}z}{\int_{z=0\mathrm{m}}^{z=2600\mathrm{m}} (\mathrm{TA}(t,z) - \mathrm{TA}_{\mathrm{ref}}(t,z))\ \mathrm{d}z} \ (\cdot\ 100\ \%) \tag{5}$$

In Figure (11) the different efficacies are shown for the scenarios with moderate OAE intensities only, since the variations are similar between the different OAE intensities. The only exception is the extreme OAE, where the efficacy becomes zero in case of PIC precipitation and the subsequent export of PIC, which is documented hereafter separately. The main points that can be recognized from Figure (11) are as follows:

- The maxima in efficacy achieved differ between the two climate scenarios, 69.3 % in SSP126 and 80.5 % in SSP370 respectively. The maximum is approached earlier in the SSP126 climate scenario than in SSP370. The maxima are always reached within A2 (area of no alkalinity deployment, black lines), but also within A1 in case of annual OAE (magenta lines). This clarifies that the lowest frequency (annual OAE) provides sufficient time for CO_2 to enter the ocean to reach equilibrated conditions before the next OAE event occurs.

- The largest fluctuations in efficacy are associated with the annual deployment scenarios, between less than 1 % at times of alkalinity addition and closely approaching the maximum efficacy about 6 – 8 months later. The lowest fluctuations happen if alkalinity is added monthly (red lines). The monthly addition also shows the lowest overall efficacy within the deployment area (around 20 %). This demonstrates that the CO_2 influx within A1 never leads to equilibrated conditions between the deployment events and most CO_2 is actually taken up outside of A1. Also, no fully equilibrated conditions are reached in case of the seasonal additions (blue lines). The variational range in efficacy of the seasonal OAE is somewhat between the signals of the monthly and annual OAE.

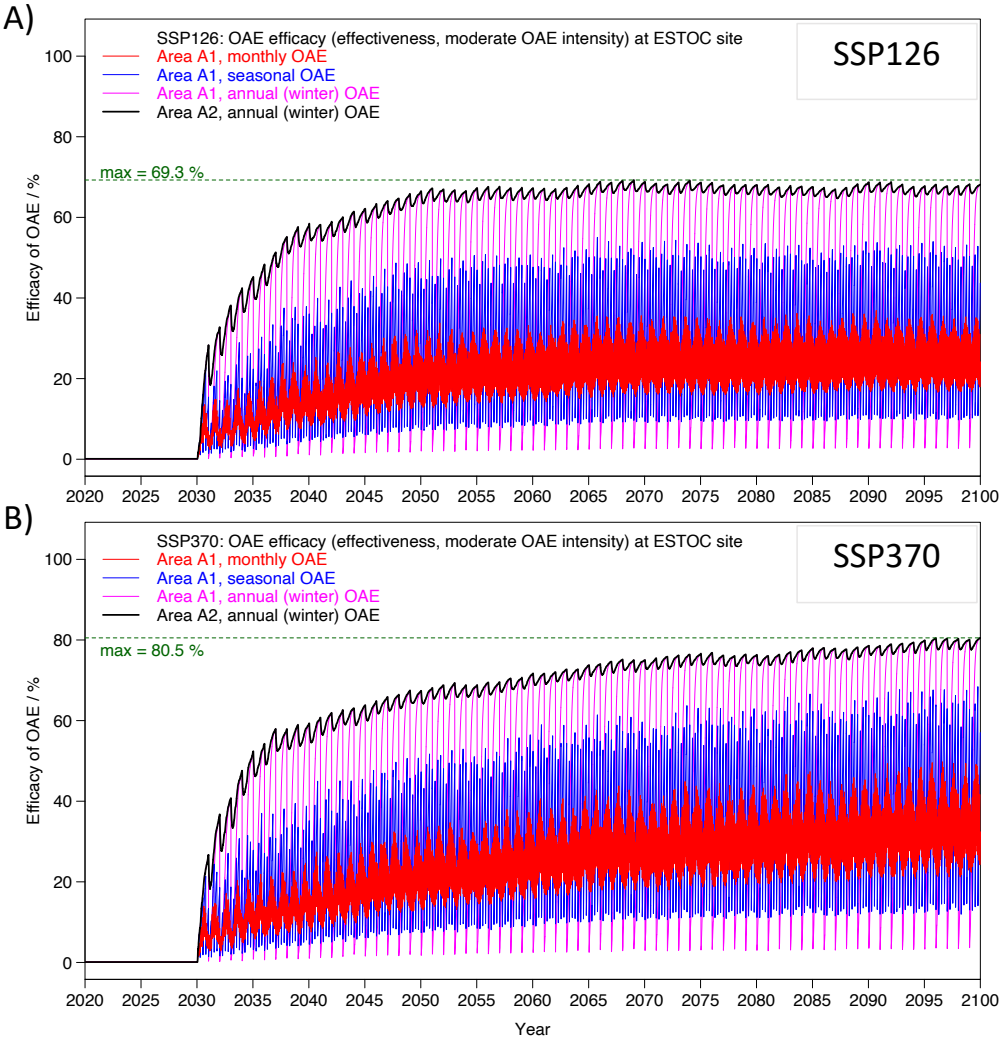

***Figure 11**: Efficacies of the different frequencies of OAE. A) Temporally resolved variations in efficacy for the climate scenario SSP126, for the area of alkalinity addition (A1), for monthly (red), seasonal (blue), and annual-winter deployments (magenta). The back line represents the efficacy of the area A2 that is not subject to alkalinity deployment, but receives alkalinity from A1 through lateral dispersion (mixing). B) Same as in A) but for the climate scenario SSP370.*

Figure (12) shows the temporal fluctuations of pH within the upper 32 m for the high intensity OAE scenario (0.2 % of total CaO available for OAE in Europe) as well as the extreme OAE scenarios (0.4 % CaO available for OAE); the latter being distinguished between deployments in winter and summer. The key messages that can be inferred from the subplots of Figure (13) are:

- The intensity of OAE determines the magnitude of the short-term pH increase, as expected. Accordingly, the monthly alkalinity additions induce the lowest perturbation in pH, not exceeding pH of 8.4 in all cases.

- Highest values, pH beyond 9, are reached after 2084 in the extreme scenario of annual-summer OAE (magenta lines). These pH values are also approached in the extreme, annual-winter deployment scenario, but more than ten years later, after 2096.

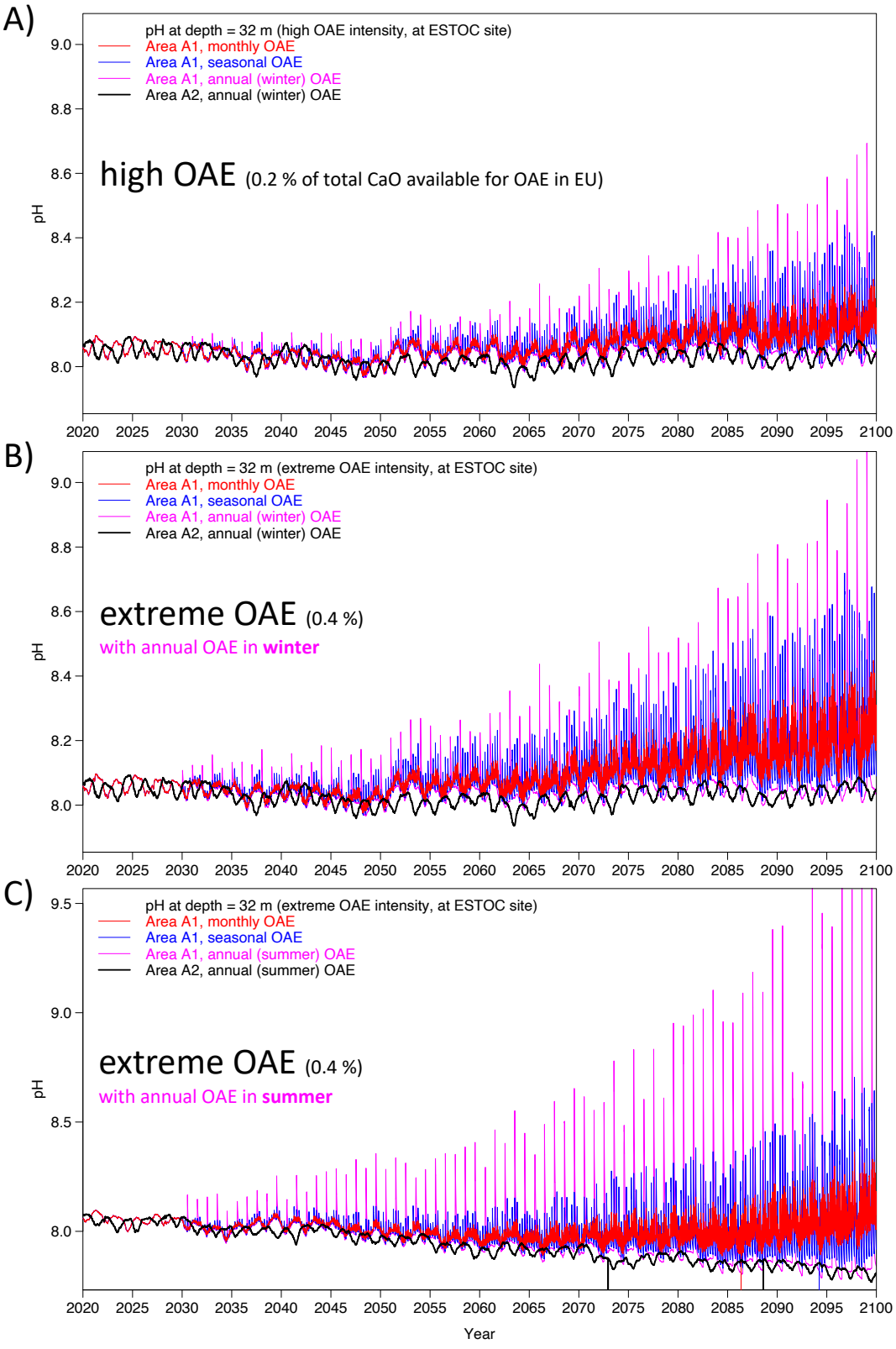

***Figure 12**: Temporal variations in pH (of SSP370), in response to different OAE scenarios (upper 32 m). A) Fluctuations in pH within area of alkalinty addition (A1), in cases of OAE of high intensity, for monthly (red), seasonal (blue), and annual-winter (magenta) deployments, as well as pH changes within the area A2 (black line). B) Same as in A), but for conditions of extreme intensity. C) As in B), but with annual-summer OAE in contrast to the annual-winter deployment scenarios.*

- The fluctuations in pH outside of the deployment area A1 are modest and largely resemble the typical seasonal variations (black lines). In the case of extreme annual-summer OAE, the pH is gradually reduced to levels lower than today's values (pH variations around 8.08) even in the A2 area, which is a continuation of the ocean acidification process of the SSP370 climate scenario. This is due the ineffective OAE because of precipitation and export of PIC, starting in the 2080's (50 years after OAE has been initiated).

After having looked at changes in efficacy and pH with high temporal resolution, we may now address the actual CDR achieved for the individual years, given the exponential increase in the availability of quicklime for OAE within Europe and the corresponding changes in alkalinity. The results of the following analysis are related to CO_2 emission per-capita in the EU, which has been approximated to be 6.25 tons CO_2 per in the year 2021 (Crippa et al., 2022). Note that these estimates do vary, depending on the underlying assumptions. The exact value may not be critical here. It is simply used as a reference baseline of total CO_2 emissions of a medium-sized city with a population of 50 000 people. This way the years are determined at which the level of CDR becomes as high as 0.3125 (Mtons CO_2) yr^{-1}, which are given in Table (2).

Figure (13) depicts the CDR of the individual years for the four different intensities of OAE as well as for the different frequencies of OAE. In this analysis the CDR of both regions, A1 and A2 together, are accounted for, while considering the respective dimensions of the two areas. The general exponential increase in CDR largely reflects the exponential total increase in CaO available for OAE, with the differences in intensity depending on the actual fraction of CaO used for the ESTOC site, from 0.05 % (low) up to 0.4 % (extreme) of the total CaO available for OAE in Europe. The year-to-year fluctuations can be attributed to the interannual variability in the ocean conditions, e.g. in vertical mixing. The most important features of this analysis are summarized below:

- On annual scale, and by looking at the combined CDR of A1 together with A2, the frequency of OAE does not matter. Regardless of the frequency, the level of CDR depends mainly on the intensity of OAE. However, the actual CDR achieved for the OAE prescribed, vary between the climate scenarios, with CDR in the SSP370 being more effective than in the SSP126. This could already be inferred from the differences found in the maxima of the efficacies shown before.

- A CDR that is equivalent to the reference line, of 0.3125 (Mtons CO_2) yr^{-1}, is not approached for the low intensity scenario within the years before 2100, which indicates that such low OAE may not be particularly effective.

- By the year 2100, the extreme OAE scenarios approach levels at which between 1.5 and slightly more than 2 Mtons CO_2 yr^{-1} could be removed from the atmosphere. The years where CDR exceeds 0.3125 (Mtons CO_2) yr^{-1} are 2059 in SSP370, and three years later in SSP126, 29 and 32 years after the initiation of the OAE.

- For the moderate intensity, which is ¼ of the extreme intensity, the year of CDR compensating the CO_2 emission of a city with 50 000 inhabitants in the EU, is reached by 2088, which is almost 30 years later than in the extreme case

- There is one particular exception where the annual CDR values fall sharply, see dashed blue line that include the annual-summer deployments of extreme intensities. This drop occurs in both climate scenarios SSP126 and SS370. This strikingly different result can be attributed to the occurrence of precipitation, with severe consequences for the CDR, with a reduced air-sea flux of CO_2. The fact that the CDR effect does not go down to zero may also come as a surprise, but this is due to the fact that alkalinity is now imported from the sides of A2 into A1; a reverse lateral transport of alkalinity so to speak.

The special case of precipitation, which ultimately prevents local OAE to become effective, will be described hereafter.

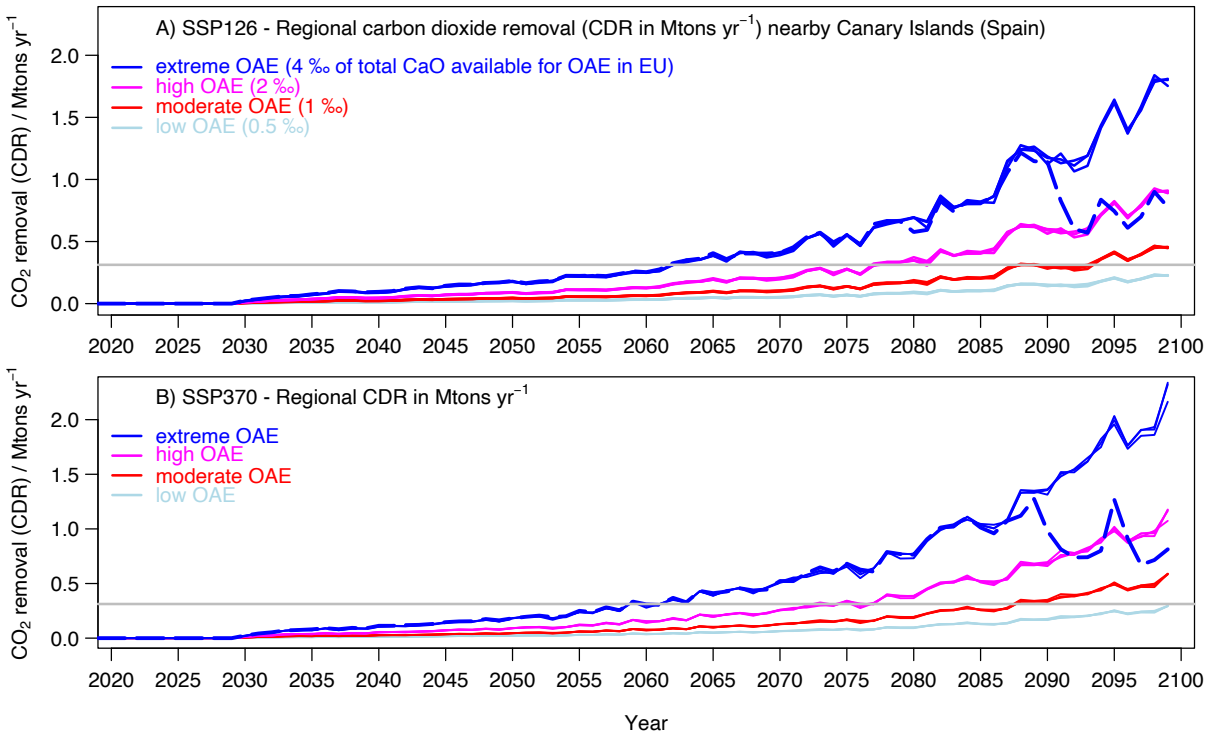

Figure 13: Carbon dioxide removal (CDR) for the different OAE scenarios. A) CDR simulation results of the SSP126 climate scenario for different OAE scenarios, for areas A1 and A2 combined: all frequencies of OAE of extreme (blue lines), high (magenta), moderate (red), and low (lightblue) intensities. B) Same as A0, but for the SSP370 climate scenario. The gray line represents the level of CO_2 emissions of a medium-sized city with a population of 50 000 people in the EU (0.3125 (Mtons CO_2) yr^{-1}.

Table 2: Compensation years by climate and alkalinity addition scenarios

Projection intensity	Frequency			
	monthly	seasonal	annual: summer	annual: winter
SSP126				
low	(n.a. = not achieved)	n. a.	n. a.	n. a.
moderate	2094	2089	2088	2088
high	2078	2078	2077	2078
extreme	2062	2062	2062	2063
SSP370				
low	n. a.	n. a.	n. a.	n. a.
moderate	2088	2088	2088	2088
high	2075	2075	2073	2075
extreme	2059	2059	2059	2059

3.2 Potential effects of precipitation (abiotic formation and export of PIC)

As explained above, the simulations of extreme intensity OAE, with an annual deployment in summer (annual-summer), exhibit solutions where precipitation occurs because the prescribed critical threshold of $\Omega_a = 7$ is exceeded. In fact, this happens not only in the case of annual summer deployment under extreme conditions but also when the intensity of OAE is high (Figure 14).

Figure (14) documents the raise in PIC concentration in response to the onset of precipitation. Some first rapid increase in PIC concentration is found in the high intensity simulation in 2091, without severe consequences with respect to OAE and thus CDR. The raise in PIC concentration remains low during the summer OAE events. These events are of short duration and are accompanied by a compensatory horizontal influx of alkalinity, which is responsible for precipation to stop, and PIC concentrations are not higher than 15 mmol m^{-3} (Figure 14A). Under conditions of an extreme OAE, the of saturation state ⍵a not only exceeds a value of 7 but raises up to values greater than 10, even reaching levels above 12. In such situation, the possible compensatory effect due to a lateral influx is insufficient and PIC formation continues, leading to PIC concentrations that are greater than 500 mmol m^{-3} (approximately 33 times higher than under the high OAE scenario). First events of PIC precipitation occur already in the year 2072 in the SSP126 climate scenario, which is earlier than in the SSP370, where 2074 is found to be the first year of significant precipitation (Figure 15). Whether this temporal difference can be related to differences in physical boundary conditions has to be still investigated. Figure (15A) highlights the impact on the DIC taken up, dropping to zero within the site of deployment. Some decrease in overall CO_2 uptake, albeit small, is then also simulated for the area A2, outside the area of alkalinity addition. Figures (15B and C) illustrate the sinking of PIC to depth, transporting the added alkalinity from the surface to much greater depths and thus eliminating CDR. It appears as if this process is more pronounced in the SSP126 climate scenario, possibly because of the lower gradient of CO_2 between the atmosphere and the surface ocean layer.

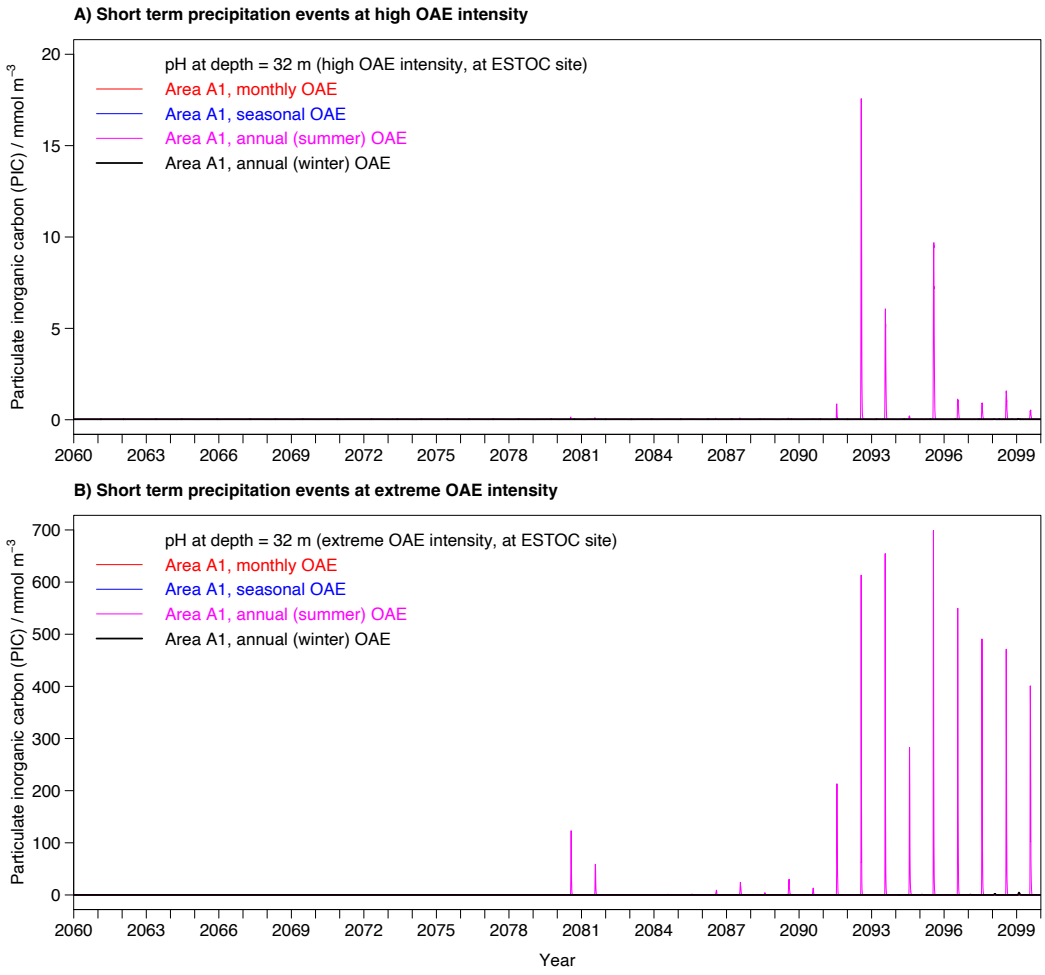

***Figure 14**: Concentration of PIC within the upper ocean layers in case of precipation. A) Raise in particulate inorganic carbon (PIC) concentration within the upper 32 m as obtained in the simulation of annual-summer OAE with high intensity. B) Same as in A) but showing the results of the OAE scenario with extreme intensity.*

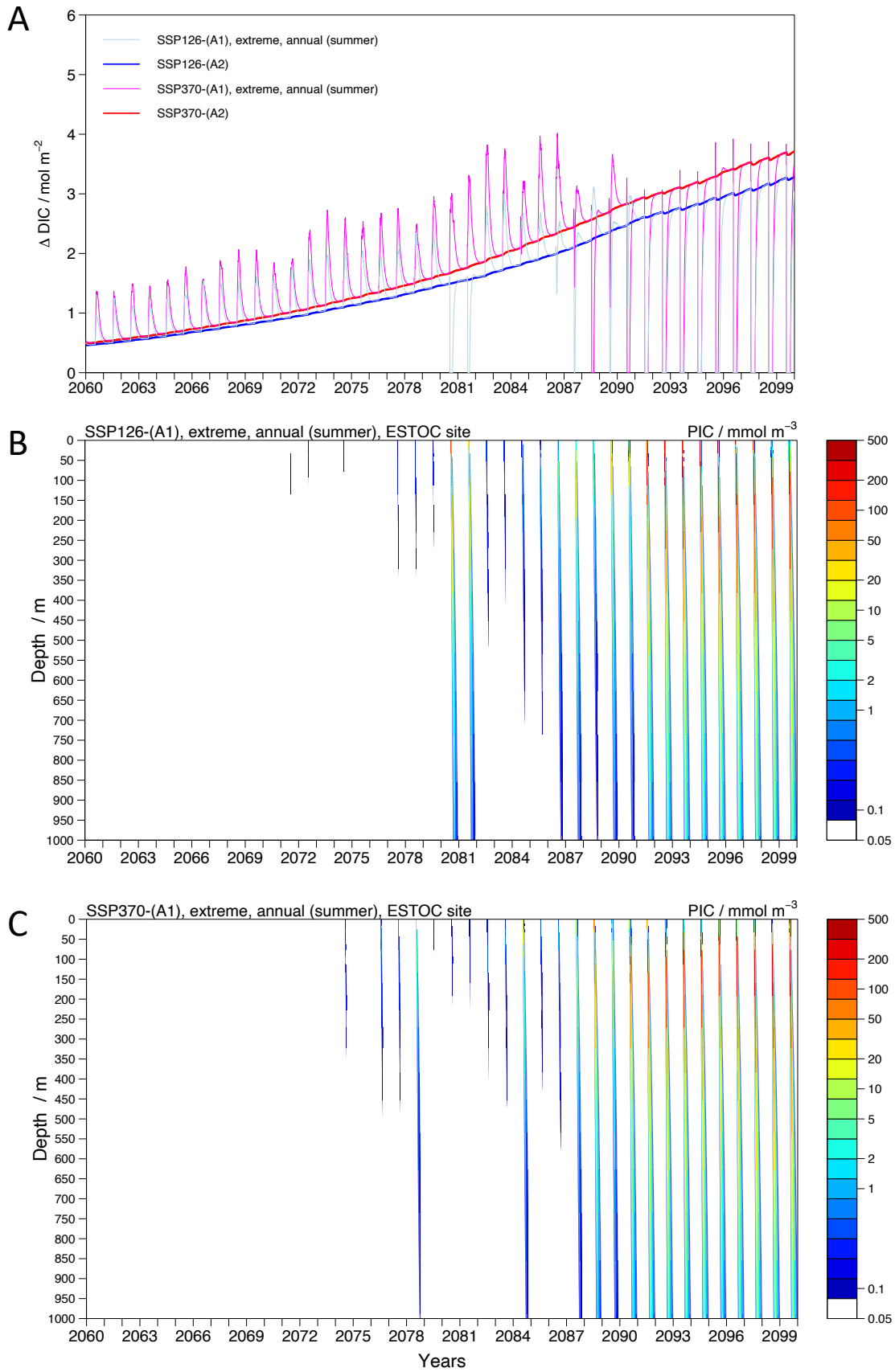

Figure 15: Changes in CO_2 uptake in association with precipitation of PIC. A) Temporal changes in integrated dissolved inorganic carbon (DIC), representing the uptake of CO_2 in the area A1 of alkalinity deployment (for SSP126, lightblue; SSP370, magenta). The changes within A2 (away from deployment site) are marked as thicker lines (SSP126 in blue, and SSP370 in red). B) and C) document the vertical export of PIC in A1 for the respective climate scenarios SSP126 and SSP370.

3.3 Potential effects of pulsed OAE on growth of phyto- and bacterioplankton

Under oligotrophic conditions the overall primary production rates are low, and much of the productivity happens at depths below 50 m where irradience is low but nutrients are mixed in from below. Due to the generally low amounts of biomass within the upper water column, the light can reach great depths and thus ensure significant primary production rates even at depths of 120 m. Generally, a large part of the production takes place at depths where the influence of a disturbance, such as that due to OAE, should only be weakly pronounced. This interpretation is further substantiated by the model results, provided that the most important potential responses can actually be represented by the model. In general, the effect of OAE on the productivity of phytoplankton, bacteria and zooplankton in the larger area A2 is marginal. Effects are hardly conceivable within A2. Therefore, results only within A1 and only for the upper perturbed layers are shown in Figures (16) and (17) that resolve the relative changes in carbon biomass of the phytoplankton, bacteria, and the zooplankton, for OAE with high and extreme intensities.

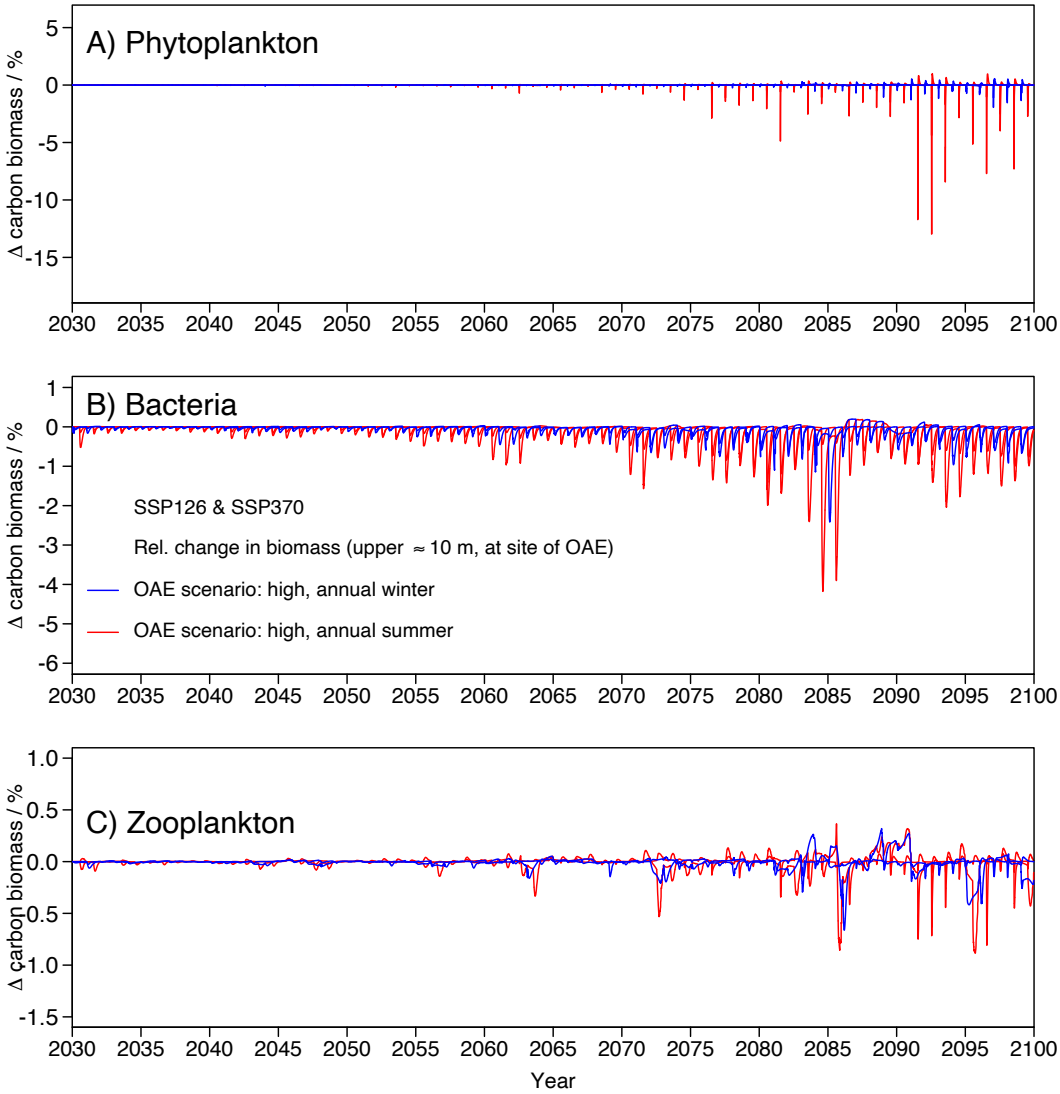

*Figure 16: Changes of plankton biomass in response to annual OAE with **high** intensity . A) Relative changes in phytoplankton carbon biomass, averaged for the two climate scenarios SSP126 and SSP370, distinguished by annual-winter (blue line) and annual-summer (red line) OAE. B) Similar relative changes as in A), but of the bacterioplankton, with adjusted scale. C) Similar relative changes as in A) and B), but of the zooplankton, with a further reduced scale on the y-axis.*

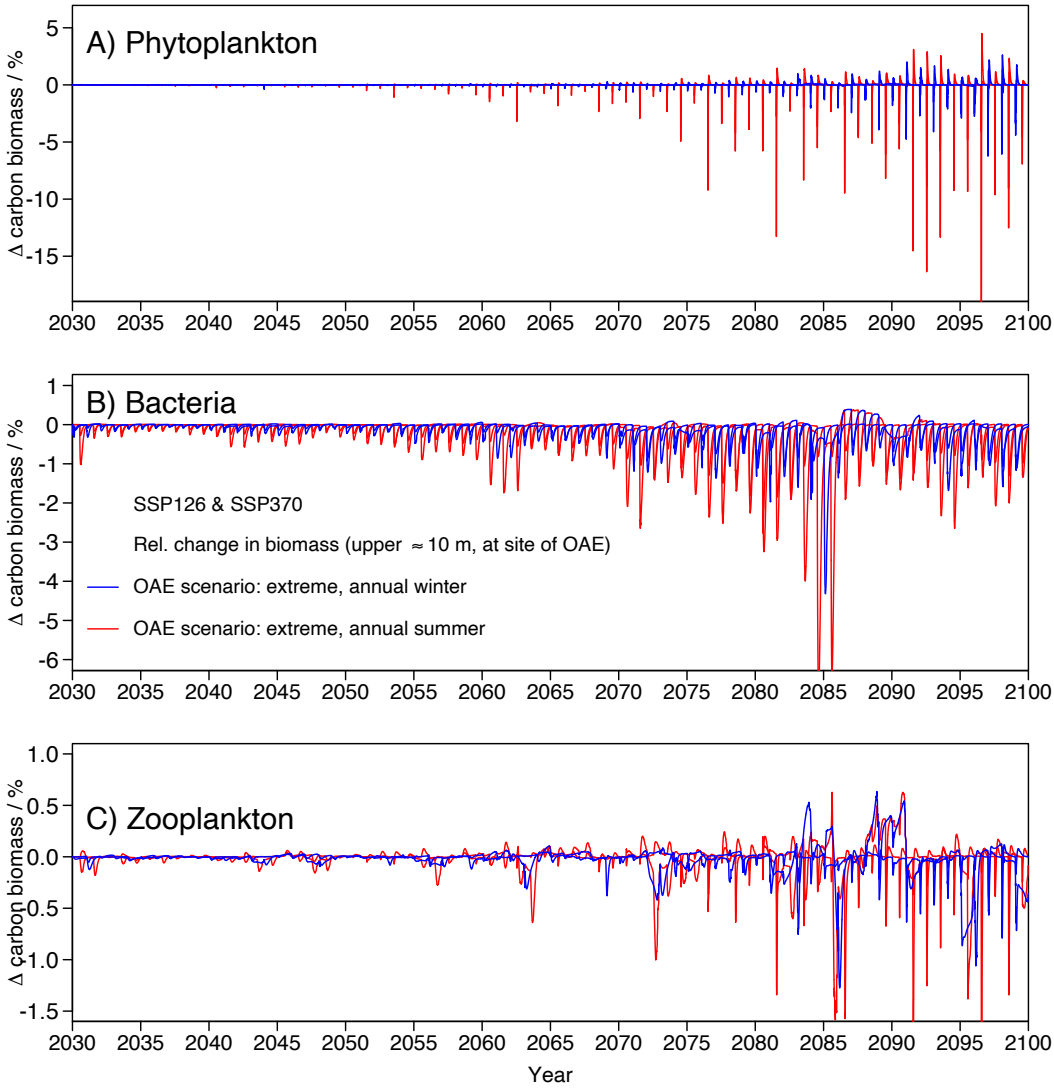

*Figure 17: Changes of plankton biomass in response to annual OAE with **extreme** intensity. A) Relative changes in phytoplankton carbon biomass, averaged for the two climate scenarios SSP126 and SSP370, distinguished by annual-winter (blue line) and annual-summer (red line) OAE. B) Similar relative changes as in A), but of the bacterioplankton C) Similar relative changes as in A) and B), but of the zooplankton. The scales of the y-axes (% change) are identical with those depicted in Figure (16).*

The key findings from the analysis of the relative changes in carbon biomass are:

- As expected, the relative changes are higher under the OAE conditions with increased intensity. The responses in phytoplankton biomass are more pronounced than in the bacterioplankton and zooplankton, showing an increase as the intensity in OAE raises with time. This general behaviour is also expressed in the relative changes of the zooplankton biomass. In contrast, the largest impact on bacteria is found for the years 2084 and 2085, which is associated with maxima that occur already in the reference solution, which can be seen in Figure (10B).

- The ranges of the responses to OAE differ between the plankton types. Relative changes up to -15 % are possible for the phytoplankton, whereas bacteria and zooplanton responses are around -6 and -1.6 % respectively. The ranges seen in the responses are sensitive to the

time of the annual alkalinity addition, with winter deployments being less harmful than the summer deployments, which corresponds to the variations seen in pH (see Figure 12)

- The negative anomalies (reductions of biomass) shortly after the OAE events are followed by some positive anomalies (higher biomass than in the reference solutions). In all cases such positive anomalies exist, but they overall impact appears to be asymmetric, e.g. with negative anomalies close to -15 % in the phytoplankton followed by a positive anomaly of only 5 %. The response patterns, and thus asymmetries seen, become less systematic in the bacteriaplankton and zooplankton, if compared with the phytoplankton responses. The anomalies in zooplankton are the least systematic and they vary over periods of years rather than on a seasonal scale. This may result from complex grazing and growth interdependencies that need to be analysed in more detail.

Figure (18) provides some insight to the typical time scales involved during and after the OAE events. To exemplify the different response behaviours in time of the plankton, anomalies are illustrated for one selected year (2089). Two responses, annual OAE in winter and in summer respectively, are looked at. Clearly, the summer responses are stronger than in winter. The negative anomalies in phytoplankton biomass induced by OAE have a duration between 1 to 2 weeks, which corresponds to the characteristic time scale of phytoplankton growth. Interestingly, the subsequent positive anomaly is less strong but stretches over a time period of about 4 weeks. Ultimately, the disturbance in phytoplankton growth only extends over a period between 1 and 2 months. The anomaly pattern becomes stretched over a period of 4 to 5 months when looking at the bacteria. The picture becomes even more complex for the anomalies seen in the zooplankton biomass. At first sight, the negative anomaly follows naturally the negative anomaly of the phytoplankton. However, the duration of the subsequent positive anomaly is prolonged to such an extent that it is still present at the time of the next OAE event. These shifts and asymmetries in the response patterns deserve closer examination, even if their magnitudes are only small. Within the scope of this deliverable, it was no longer possible to achieve this in time.

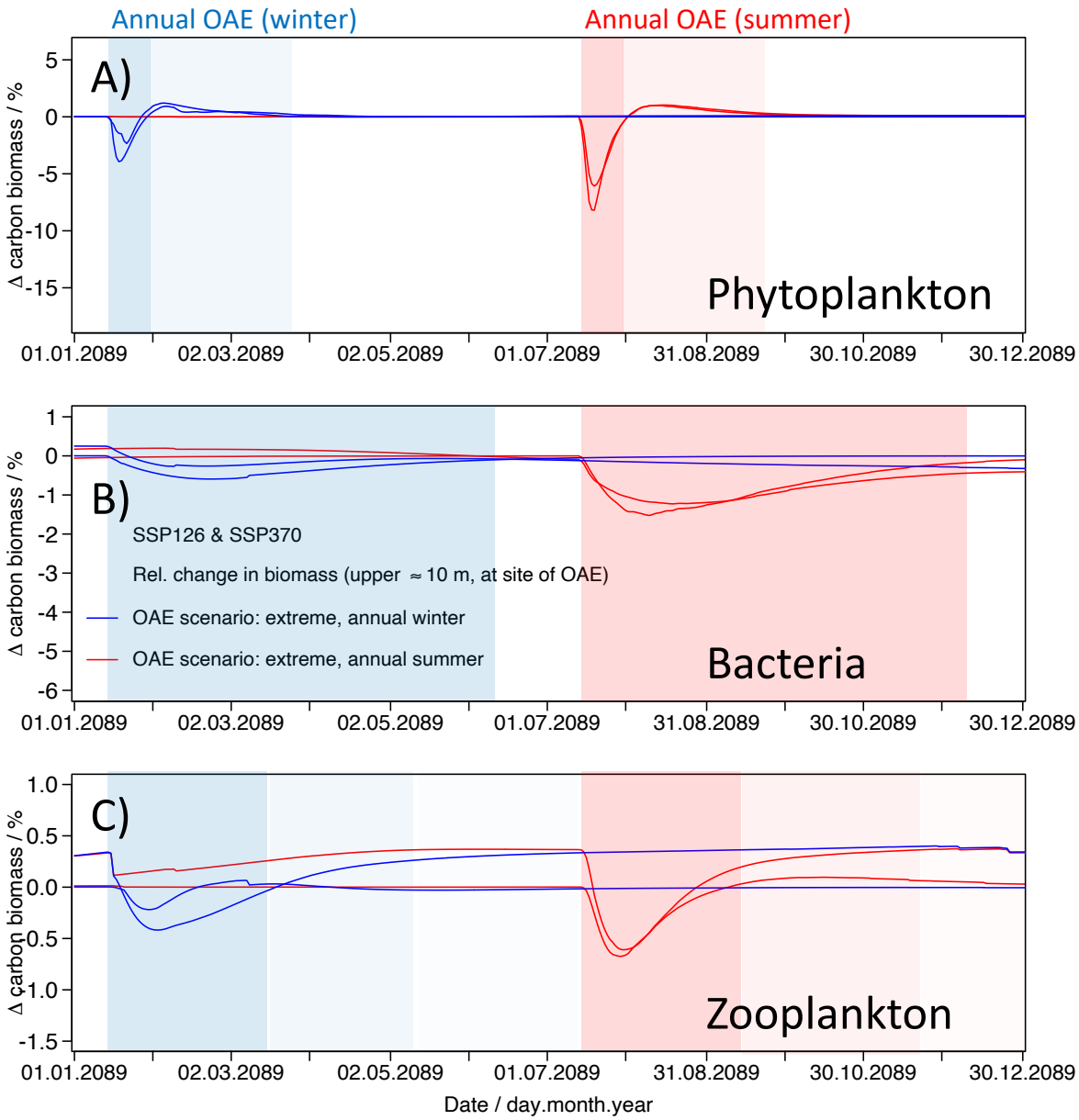

***Figure 18**: Time scales of the response patterns in association with annual OAE scenarios. A) Anomalies, relative changes in phytoplankton biomass in %, induced by annual winter (blue lines) and summer (red lines) OAE with extreme intensity for SSP126 and SSP370. B) Same as in A) but for the bacteria, with a refined scale of the y-axis. C) Same as in A) and B) but for the zooplankton biomass, with a further refined scale of the y-axis.*

4. Conclusion

The model simulations analysed in this study offer new insights into the quantitative connections between the intensity and frequency of OAE in an oligotrophic region and their impacts on the induced broader CDR in a larger area surrounding the site of alkalinity addition. On local scale, where OAE takes place, short-term perturbations of the carbonate system can be strong, with local raise in pH that can exceed values of 9. Despite these considerable local, short-term increase in pH, the simulation results show that the negative effects on the growth and biomass of phytoplankton,

bacteria and zooplankton are generally low, based on the growth response parameterizations introdued to the model. The most important conclusions that can be drawn from this study are:

- **Parameterization of the growth response of phyto- and bacterioplankton to variations of the carbonate system**: Amongst the two response functions under consideration, based on either Bach et al. (2015) or on Paul and Bach (2020), the relationship of Bach et al. (2015) caused instabilities in simulated growth rates of the phytoplankton, and not all OAE scenario could be evaluated in the end. The relationship proposed by Paul and Bach (2020) turned out to be a more robust response function and appears to be better applicable for similar simulations of pulsed OAE in large-scale or global ocean biogeochemical models. The newly introduced parameterization of the bacterial growth response to variations in pH is effective and stable, and may even be used for simulations of ocean acidification effects.

- **Different intensities of OAE**: The four different intensities considered for this analysis were derived from the total potential amount of quicklime (CaO) available for OAE in Europe upt to the year 2100, starting with OAE in 2030. The low intensity scenarios (0.05 % of available CaO) were too low to approach some CDR until 2100 that is as high as the annual emission of a city with 50 000 inhabitants (0.3125 (Mtons CO_2) yr^{-1}) within the EU. With an intensity of 0.4 % of available CaO for local OAE, a considerable portion of CDR can be achieved; an intensity with which the 0.3125 (Mtons CO_2) yr^{-1} are approach in the years 2059 (SSP370) and 2062 (SSP126), 29 and 32 years after the initiation of the local OAE.

- **Different frequencies of OAE**: The four different frequencies of OAE did not affect the efficacy and thus CDR within the larger area (A2). The main temporal effects of the various frequencies are expressed in the area in which the OAEs are actually realized. If OAE happens on a monthly basis, the maxima in efficacy evaluated locally are around 20 %. This means that most of the additional CO_2 uptake actually occurs outside of the area of OAE. In cases of seasonal OAE the local efficacy remains below approximately 60%. In contrast, the annual OAE introduces efficacies close to zero at times of alklainity addition, but then reach the maximum before the next OAE event. Thus, annual OAE would facilitate local monitoring of the effectiveness of OAE, while the effectiveness of monthly and seasonal OAE is unlikely to be correctly determined at the local site of OAE. However, as shown here, annual OAE can be associated with the risk of reaching high pH values and high levels of the aragonite saturation state and the risk of precipitation (formation and export of PIC).

- **PIC precipitation**: Only in the extreme OAE scenario with annual alkalinity addition during the summer periods, the imposed critical aragonite saturation state of $\Omega_a = 7$ initiated precipitation that causes CDR to stop locally. In these simulations, even values greater than $\Omega_a = 12$ are obtained. However, the simulations with extreme OAE intensities but with annual alkalinity additions during the winter period, when vertical mixing reaches greater depths, do not induce significant precipitation in the model solutions.

Apart from a too large amount of alkalinity addition, prior knowledge about the mixing depth at times of OAE is critical if precipitation is to be avoided.

- **Responses in the plankton**: The responses in plankton growth and distribution of biomass are only expressed at (or nearby) the site of OAE. Within the larger surrounding area resolved by the model, the effects are harldy noticeable, because of the lateral dispersion. The major perturbations are restricted to the upper water column. The model results of the high and extreme annual-winter OAE scenarios reveal relative reduction in carbon biomass to be less than 15 % in the phytoplankton, no more than 5% in the bacteria, and less than 1.5 % in zooplankton biomass. These periods of reduced growth and thus decreased biomass concentrations are followed by prolonged periods of growth where the biomass increases again. According to the model results, the time scales of recovery of the phytoplankton are one to two weeks. Interestingly, although not fully analysed and understood, the time scales of recovery seen in the bacteria and zooplankton are much longer, rather months than weeks. This indicates that even short-term perturbations, as e.g. induced by the annual OAE, may cause, albeit very small, effects on the development of the bacteria and zooplankton over some prolonged period.

5. References

Bach, Lennart Thomas, Ulf Riebesell, Magdalena A. Gutowska, Luisa Federwisch, and Kai Georg Schulz. "A unifying concept of coccolithophore sensitivity to changing carbonate chemistry embedded in an ecological framework." *Progress in Oceanography* 135 (2015): 125-138.

Bach, Lennart Thomas. "The additionality problem of ocean alkalinity enhancement." *Biogeosciences* 21 (2024): 261-277.

Bergmann, Tommi, et al. "CO2 Removal Potential of Two Ocean-based NETs in Earth System Models in a Realistic Deployment Scenario." *EGU General Assembly 2024.* Vienna: https://doi.org/10.5194/egusphere-egu24-18363, 2024, 14-19 Apr 2024.

Bisswanger, Hans. "Enzyme assays." *Perspectives in Science* 1 (2014): 41-55.

Caserini, Stefano, et al. "Potential of Maritime Transport for Ocean Liming and Atmospheric CO2 Removal." *Frontiers in Climate* 3 (2021): 575900.

Cianca, Andrés, Peer Helmke, Beatriz Mouriño, María José Rueda, Octavio Llinás, and Susanne Neuer. "Decadal analysis of hydrography and in situ nutrient budgets in the western and eastern North Atlantic subtropical gyre." *Journal of Geophysical Research* 112 (2007): C07025.

Crippa, M, et al. "CO2 emissions of all world countries – JRC/IEA/PBL 2022 Report." Publications Office of the European Union, Luxembourg, 2022.

González-Dávila, M, J M Santana-Casiano, M J Rueda, and O Llinás. " The water column distribution of carbonate system variables at the ESTOC site from 1995 to 2004." *Biogeosciences*, no. 7 (2010): 3067-3081.

Grossowicz, Michal, and Markus Pahlow. "Zooplankton seasonal vertical migration in an optimality-based plankton ecosystem model." *Journal of Plankton Research*, 2024 (in press).

Hartmann, Jens, et al. "Stability of alkalinity in ocean alkalinity enhancement (OAE) approaches – consequences for durability of CO2 storage." *Biogeosciences* 20 (2023): 781-802.

Moras, Charly A, Lennart T Bach, Tyler Cyronak, Renaud Joannes-Boyau, and Kai G Schulz. "Ocean alkalinity enhancement - avoiding runaway CaCO3 precipitation during quick and hydrated lime dissolution." *Biogeosciences* 19 (2022): 3537-3557.

Neuer, Susanne, et al. "Biogeochemistry and hydrography in the eastern subtropical North Atlantic gyre. Results from the European time-series station ESTOC." *Progress in Oceanography* 72 (2007): 1-29.

O'Neill, Brian C., et al. "The Scenario Model Intercomparison Project (ScenarioMIP) for CMIP6." *Geoscientific Model Developent* 9 (2016): 3461-3482.

Oschlies, Andreas, et al., . *Guide to Best Practices in Ocean Alkalinity Enhancement Research (OAE Guide 23).* Copernicus Publications, State Planet, 2023.

Pahlow, Markus, Heiner Dietze, and Andreas Oschlies. "Optimality-based model of phytoplankton growth and diazotrophy." *MARINE ECOLOGY PROGRESS SERIES* 489 (2013): 1-16.

Paul, Allanah, and Lennart T Bach. "Universal response pattern of phytoplankton growth rates to increasing CO2." *New Phytologist* 228 (2020): 1710-1716.

Piontek, Judith, Martin Sperling, Eva-Maria Nöthig, and Anja Engel. "Multiple environmental changes induce interactive effects on bacterial degradation activity in the Arctic Ocean." *Limnology and Oceanography* 60 (2015): 1392-1410.

Riahi, Keywan, et al. "The Shared Socioeconomic Pathways and their energy, land use, and greenhouse gas emissions implications: An overview." *Global Environmental Change* 42 (2017): 153-168.

Seifert, Miriam, Cara Nissen, Björn Rost, and Judith Hauck. "Cascading effects augment the direct impact of CO2 on phytoplankton growth in a biogeochemical model." *Elementa Science of the Anthropocene* 10, no. 1 (2022).

Yumruktepe, Veli Çağlar, Barış Salihoğlu, and Susanne Neuer. "Controls on carbon export in the subtropical North Atlantic." *Progress in Oceanography* 187 (2020): 102380.

Zhurbas, Victor, Dmitry Lyzhkov, and Natalia Kuzmina. "Drifter-derived estimates of lateral eddy diffusivity in the World Ocean with emphasis on the Indian Ocean and problems of parameterisation." *Deep-Sea Research I* 83 (2014): 1-11.